2020-12

DEVELOPMENT OF A MULTISTAGE ROCKET TEST PLATFORM TO DELIVER CUBESAT FORM FACTOR TO NEAR-SPACE ALTITUDES

Brandt, Camron A.

Monterey, CA; Naval Postgraduate School

NAVAL POSTGRADUATE SCHOOL

MONTEREY, CALIFORNIA

THESIS

DEVELOPMENT OF A MULTISTAGE ROCKET TEST PLATFORM TO DELIVER CUBESAT FORM FACTOR TO NEAR-SPACE ALTITUDES

by

Camron A. Brandt

December 2020

Thesis Advisor:	James H. Newman
Co-Advisor:	Dillon Pierce, Deputy Commandant for Combat Development
Second Reader:	Christopher M. Brophy

THIS PAGE INTENTIONALLY LEFT BLANK

REPORT DOCUMENTATION PAGE			*Form Approved OMB No. 0704-0188*

1. AGENCY USE ONLY *(Leave blank)*	**2. REPORT DATE** December 2020	**3. REPORT TYPE AND DATES COVERED** Master's thesis

4. TITLE AND SUBTITLE DEVELOPMENT OF A MULTISTAGE ROCKET TEST PLATFORM TO DELIVER CUBESAT FORM FACTOR TO NEAR-SPACE ALTITUDES	**5. FUNDING NUMBERS**
6. AUTHOR(S) Camron A. Brandt	
7. PERFORMING ORGANIZATION NAME(S) AND ADDRESS(ES) Naval Postgraduate School Monterey, CA 93943-5000	**8. PERFORMING ORGANIZATION REPORT NUMBER**
9. SPONSORING / MONITORING AGENCY NAME(S) AND ADDRESS(ES) N/A	**10. SPONSORING / MONITORING AGENCY REPORT NUMBER**

11. SUPPLEMENTARY NOTES The views expressed in this thesis are those of the author and do not reflect the official policy or position of the Department of Defense or the U.S. Government.

12a. DISTRIBUTION / AVAILABILITY STATEMENT Approved for public release. Distribution is unlimited.	**12b. DISTRIBUTION CODE** A

13. ABSTRACT (maximum 200 words)

The Naval Postgraduate School (NPS) Small Satellite Lab places heavy emphasis on the research, development, and integration of emerging technologies on future spacecraft. An integral part of the advancement of these technologies is the ability to test them in real-world environmental conditions. CubeSats remain a viable choice for rapid prototyping and proof-of-concept testing. Delivering CubeSats to near-space environments is a method of demonstrating the feasibility of these new technologies. Amateur high-power rocketry offers an additional platform to augment the already existing high-altitude balloons by delivering payloads containing the new technologies and CubeSat form factor small satellites to near-space environments. Previous NPS research has produced a single stage high-power rocket capable of attaining an approximate altitude of 11.9 km (39,000 feet) above ground level. This thesis applies optimal control theory to develop a multi-stage rocket capable of altitudes in excess of what was previously reached by both high-altitude balloons and the previously designed high-power rocket.

14. SUBJECT TERMS rocket, CubeSat, high-altitude balloon, Small Satellite Lab	**15. NUMBER OF PAGES** 83
	16. PRICE CODE

17. SECURITY CLASSIFICATION OF REPORT	**18. SECURITY CLASSIFICATION OF THIS PAGE**	**19. SECURITY CLASSIFICATION OF ABSTRACT**	**20. LIMITATION OF ABSTRACT**
Unclassified	Unclassified	Unclassified	UU

NSN 7540-01-280-5500 Standard Form 298 (Rev. 2-89) Prescribed by ANSI Std. 239-18

THIS PAGE INTENTIONALLY LEFT BLANK

Approved for public release. Distribution is unlimited.

DEVELOPMENT OF A MULTISTAGE ROCKET TEST PLATFORM TO DELIVER CUBESAT FORM FACTOR TO NEAR-SPACE ALTITUDES

Camron A. Brandt
Lieutenant, United States Navy
BS, Iowa State University, 2013

Submitted in partial fulfillment of the
requirements for the degree of

MASTER OF SCIENCE IN ASTRONAUTICAL ENGINEERING

from the

NAVAL POSTGRADUATE SCHOOL
December 2020

Approved by: James H. Newman
Advisor

Dillon Pierce
Co-Advisor

Christopher M. Brophy
Second Reader

Garth V. Hobson
Chair, Department of Mechanical and Aerospace Engineering

THIS PAGE INTENTIONALLY LEFT BLANK

ABSTRACT

The Naval Postgraduate School (NPS) Small Satellite Lab places heavy emphasis on the research, development, and integration of emerging technologies on future spacecraft. An integral part of the advancement of these technologies is the ability to test them in real-world environmental conditions. CubeSats remain a viable choice for rapid prototyping and proof-of-concept testing. Delivering CubeSats to near-space environments is a method of demonstrating the feasibility of these new technologies. Amateur high-power rocketry offers an additional platform to augment the already existing high-altitude balloons by delivering payloads containing the new technologies and CubeSat form factor small satellites to near-space environments. Previous NPS research has produced a single stage high-power rocket capable of attaining an approximate altitude of 11.9 km (39,000 feet) above ground level. This thesis applies optimal control theory to develop a multi-stage rocket capable of altitudes in excess of what was previously reached by both high-altitude balloons and the previously designed high-power rocket.

THIS PAGE INTENTIONALLY LEFT BLANK

TABLE OF CONTENTS

THIS PAGE INTENTIONALLY LEFT BLANK

LIST OF FIGURES

LIST OF TABLES

THIS PAGE INTENTIONALLY LEFT BLANK

LIST OF ACRONYMS AND ABBREVIATIONS

AGL	above ground level
COTS	commercial-off-the-shelf
DIDO	MATLAB optimal control toolbox
HAB	high-altitude balloon
HEE	Hamiltonian evolution equation
HMC	Hamiltonian minimization condition
HVC	Hamiltonian value condition
KKT	Karush-Kuhn-Tucker
MSL	mean sea level
NPS	Naval Postgraduate School
OCP	optimal control problem

THIS PAGE INTENTIONALLY LEFT BLANK

ACKNOWLEDGMENTS

I would first and foremost thank my family, without whose support none of this would have been possible. Secondly, I would like to thank my advisory team, Dr. James Newman, Capt. Dillon Pierce, and Dr. Christopher Brophy: your guidance and instruction were instrumental to the successful completion of this thesis. Next, I would like to thank Dr. Mark Karpenko, for without your assistance I could not have completed the two-stage rocket problem. Lastly, I would like to thank all the friends I have made throughout the completion of this program.

THIS PAGE INTENTIONALLY LEFT BLANK

I. INTRODUCTION AND BACKGROUND

A. MOTIVATION

The Small Satellite (SmallSat) Lab at the Naval Postgraduate School (NPS) exists to provide hands-on education and research opportunities for students completing their master's degrees by researching and developing emerging technologies and their applications for future spacecraft. An integral part of the advancement of these technologies is the ability to test them in real-world environmental conditions. CubeSats remain a viable choice for prototyping and proof of concept testing. Delivering CubeSats to near-space environments is a method of quickly demonstrating the feasibility of these new technologies. Amateur high-power rocketry offers an additional platform to augment the already existing high-altitude balloon (HAB) payload delivery system. These rockets are capable of delivering payloads containing the new technologies and CubeSat form factor small satellites to near-space environments. Previous NPS research has produced a single stage high-power rocket capable of attaining an approximate altitude of 11.8 km (39,000 feet) above ground level (AGL) [1].

HABs is the generic term for the weather balloons used extensively by the SmallSat lab for testing of CubeSat-compatible technologies. HABs offer a low cost and a less complex method of testing before space flight demonstration. They have been flown at heights from a few kilometers to over 30 kilometers AGL with a typical maximum altitude of approximately 18 km (59,000 ft). As part of a directed study, a group of NPS students in 2017 flew a HAB to 35 km (115,000 ft) AGL [2]. This flight has been the maximum achieved altitude by a HAB for the SmallSat Lab. One drawback to HAB flights is that they have a slow ascent rate and thus are greatly affected by wind conditions. With a typical ascent of around 5 m/s, the possibility for large drift ranges is highly probable. This thesis seeks to augment the existing HAB program by providing an option that can achieve greater altitudes with less drift than can be achieved by a HAB. High power rockets are capable of delivering less drift due to the significantly lower time to apogee. For example, a Space Systems Academic Group (SSAG) rocket achieved its maximum altitude, 11.8 km,

in approximately two minutes whereas a HAB flight would take about 45 minutes to achieve the same maximum altitude [1], [2].

B. THESIS OBJECTIVE AND SCOPE

Previous thesis work developed a two-stage rocket design [1]. This thesis seeks to expand on this work by utilizing trajectory planning and optimal control theory to obtain a model that will be utilized to determine the maximum altitude that can be achieved by a rocket for a given propellant mass. The theory will produce the optimal thrust profile for the rocket and for a two-stage rocket the optimal stage timing. By optimizing a single stage rocket the theory can be analyzed and compared to a commercially available rocket motor. The computer algorithm that will be utilized for this research is DIDO. DIDO is a MATLAB optimal control toolbox that utilizes pseudospectral optimal control theory to solve an optimal control problem (OCP) [3]. By solving this OCP, it is possible to determine the maximum achievable altitude for a rocket based on dry mass, propellant mass, and motor characteristics. Through the use of pseudospectral knotting this optimal control theory can then be applied to a multi-stage rocket to determine the precise staging delay and thrust profile to achieve the greatest possible altitude [4]. This theoretical altitude can then be used to inform and obtain a waiver from the Federal Aviation Administration [5]. Such a waiver is required when flying high-power rockets above 18,000 feet, so an important aspect is knowing the maximum achievable altitude. Another goal of this research is to develop code that can be used to determine optimal delay time and maximum altitude for future iterations of this rocket design based on rocket size, wet and dry masses, and motor characteristics.

C. THESIS OUTLINE

The remainder of this thesis is intended to present to the reader the overall development and application of utilizing optimal control theory as applied to this research. Chapter II provides the baseline knowledge of optimal control theory. Chapter III introduces the problem and presents the development of the model utilized for the OCP. Chapter IV introduces the single stage rocket optimization problem and its solution.

Chapter V describes the multi-stage rocket problem with a focus on stage delay time. Finally, Chapter VI gives conclusions and suggested areas of future work.

THIS PAGE INTENTIONALLY LEFT BLANK

II. OPTIMAL CONTROL THEORY

The optimal control theory is defined by Ross [6] as "a branch of mathematical optimization that deals with finding a control for a dynamical system over a period of time such that an objective function is optimized." Optimal control theory has the ability to determine an optimal path given a multitude of possible design considerations. Optimal control also can apply constraints on the dynamics such as path or control constraints as well as boundary conditions. This works to allow for path "keep out" zones or control constraints such as acceleration restrictions. This theory starts by developing a cost function that will be minimized to determine the optimal path. This cost function can consist of minimum time, fuel, energy, or any other performance metric associated with the dynamics of the problem. For this thesis, the cost function minimizes the negative of the altitude, which in turn produces the maximum altitude.

A. STANDARD OPTIMAL CONTROL PROBLEM

A standard optimal control problem is presented by Ross in [6] as:

$$\begin{cases} \textit{Minimize} & J[\underline{x}(\cdot),\underline{u}(\cdot),t_f] & = E(x(t_f),t_f)+\int_{t_0}^{t_f} F(x(t),u(t),t)dt \\ \textit{Subject to} & \dot{x} & = f(x(t),u(t),t) \\ & x(t_0) & = x^0 \\ & t_0 & = t^0 \\ & e(x_f,t_f) & = 0 \end{cases} \tag{2.1}$$

In Equation 2.1, $J[\underline{x}(\cdot),\underline{u}(\cdot)]$ is the cost functional that is being minimized based on the state variables, *x*, and control variables, *u*. $E(x(t_f),t_f)$ is the endpoint cost function that is associated with the final time, such as final velocity, altitude or time. $F(x(t),u(t),t)$ is the running cost. An example of running cost is the energy used to complete a maneuver or the fuel burned and is commonly associated with the control effort. $\dot{x}=f(x(t),u(t),t)$ is the dynamics of the system that is being optimized. $x(t_0)=x^0$ and $t_0=t^0$ are the starting

conditions of the system. $e(x_f, t_f) = 0$ are the endpoint conditions applied to the system and set the final state boundary conditions.

Pontryagin's principle is defined as "Given an optimal solution $\{x(\bullet), u(\bullet), t_f\}$ to Problem P_C, there exists a costate, $\lambda(\bullet)$, and a covector, ν, that satisfies the Adjoint Equation, the Hamiltonian Minimization Condition, the Hamiltonian Value Condition, the Hamiltonian Evolution Equation and the Transversality Condition" [6]. These conditions do not explicitly solve the OCP but provide the necessary conditions that must be met for an optimal solution [6]. Once the dynamics of the system are created in state space form, $\dot{x} = f(x(t), u(t), t)$, Pontryagin's principle can be applied to develop the boundary value problem (BVP) to be solved.

B. SOLVING THE OPTIMAL CONTROL PROBLEM

The first step of solving the optimal control problem is to construct the Hamiltonian as defined in [6] for the system given by Equation 2.2

$$H(x, u, \lambda, t) = F(x, u, t) + \lambda^T f(x, u, t), \tag{2.2}$$

where F is the running cost of the system given in the cost functional, λ is the convector, a Lagrange multiplier of the state variables, and $f(x, u, t)$ is the state dynamics of the system. The Hamiltonian is the cornerstone of the OCP that the next three steps build from. The next step of solving the OCP is to apply the Hamiltonian Minimization Condition (HMC) which minimizes the Hamiltonian with respect to the control. This is defined as

$$\begin{aligned} &\min H(x, u, \lambda) \\ &u^L \le u \le u^U \end{aligned}. \tag{2.3}$$

Completing this minimization to determine the global minimum of the Hamiltonian ensures that the derived control is optimal. To complete the Hamiltonian minimization the partial derivative is taken with respect to each of the control variables, *u*, and setting them equal to zero.

$$\frac{\partial H}{\partial u} = 0 \tag{2.4}$$

In some cases, based on the problem formulation, when solving Equation 2.4 the dependence on the control, u is eliminated. When this occurs, the Lagrangian of the Hamiltonian must be developed, and the derivative defined in Equation 2.4 is taken determine the proper value for the control [6].

$$\bar{H}(\mu, \lambda, x, u, t) = H(\lambda, x, u, t) + \mu^T u \tag{2.5}$$

In Equation 2.5, μ is a Lagrange multiplier for the control. This allows the Karush-Kuhn-Tucker (KKT) Complementarity conditions to be applied to determine the proper control value. The KKT conditions are

$$\mu = \begin{cases} \leq 0 & if \quad h(x,u) = h^L \\ 0 & if \quad h^L < h(x,u) < h^U \\ \geq 0 & if \quad h(x,u) = h^U \end{cases} . \tag{2.6}$$

In Equation 2.6, $h(x,u)$ represents the path and control constraint. Next, the costates are solved using the adjoint equation given by

$$\dot{\lambda} = -\frac{\partial H}{\partial x} . \tag{2.7}$$

These costates in conjunction with the state dynamics formulate the BVP that must be solved to complete the OCP. However, depending on the number of given boundary condition there may be more unknowns than equations. For each of the N states associated with the OCP there are N costates. For this reason, there are 2N equations that need to be solved to determine a unique solution to the BVP. Thus, 2N point conditions are required for a unique solution. This requirement leads to the last step of Pontryagin's Principle, the Transversality Conditions which derives any missing point conditions that were unknown when the problem was formulated. Transversality is determined by taking the partial derivative of the Endpoint Lagrangian with respect to the final state conditions.

$$\lambda(t_f) = \frac{\partial \bar{E}}{\partial x_f} \tag{2.8}$$

$\bar{E}$ in equation 2.8 is the Endpoint Lagrangian.

$$\bar{E}(\nu, x(t_f)) = E(x(t_f)) + \nu^T e(x(t_f)) \tag{2.9}$$

Solving equation 2.8 provides the remaining required boundary conditions needed to solve the BVP.

III. OPTIMAL CONTROL MODEL DEVELOPMENT

The model used for optimal control theory utilizes varying parameters to determine the drag force on the rocket. Higher fidelity models utilize table lookups for higher accuracy in the air density model and drag coefficient while lower fidelity models utilize simplified equations or constants for these values. This chapter seeks to prove that utilizing these simplified models produces similar results to the higher fidelity models. Based on the work of Robert H. Goddard in "A Method of Reaching Extreme Altitudes" [7]. The truth model for a one-dimensional rocket ascending in the presence of drag and gravity, for a given initial and final mass is

$$\begin{aligned} \dot{r} &= v \\ \dot{v} &= \frac{u \cdot c}{m} - \frac{D(r,v)}{m} - \frac{\mu}{(r+\mathrm{R_e})^2} \\ \dot{m} &= -u \end{aligned} \tag{3.1}$$

such that

r = radius above ground level

v = velocity

m = mass of the rocket

u = mass flow rate of rocket motor (system input)

c = characteristic velocity of rocket motor

μ = Gravitational Constant

R_e = Radius of Earth

This model is based on $\sum F = ma$ and the mass is changing only with respect to the mass exiting the rocket motor and assumes a purely ballistic flight with no active guidance. The system state-vector consists of *r*, *v*, and *m*. The input (control) for the system is the mass flow rate out of the rocket motor given by the variable *u*. The drag force is modeled using the following equation.

$$D(r,v) = \frac{1}{2} C_D A v^2 \rho \tag{3.2}$$

In order to obtain a fully developed truth model the drag coefficient would need to be determined for all values of velocity because drag varies greatly based on both velocity (Mach number) and Reynolds number of the fluid [8]. For this reason, three simplified models were developed to determine the level of fidelity that produced consistent realistic results. The first model is a medium fidelity model that utilizes a variable drag coefficient and the NRLMSISE-00 atmosphere density model. The second model is a low-fidelity model that utilized a constant drag coefficient and an exponential atmosphere density and the last model is a zero-drag model. The more complex models rely on table lookups and linear interpolation for more precise data due to exact equations being unknown for higher fidelity drag and density models. These table lookups and interpolations add areas that cause the optimal control algorithm to fail and result in increased computation time. For this reason, it is important to determine the lowest possible fidelity that can achieve realistic results.

The models were simulated using a test control trajectory to determine the state trajectories of each model. For all three models MATLAB's ode45 was used to solve for the state trajectories due to its versatile ability to solve differential equations with smooth solutions. This solver was also chosen because of the ability to overload the function call to pass in needed variables. Since ode45 is a Runge-Kutta method, the function utilizes a variable time step. The simulations were run to 40 seconds due to the proximity to apogee for the higher fidelity models. Since all three models use the same dynamics equations, the same test control was utilized for all three models. The control utilized is a simulated rocket motor that fires for five seconds then burns out as depicted in Figure 1. Simulating the models with the same control trajectory allows them to be analyzed to determine if an increase in fidelity results in an appreciable increase in accuracy.

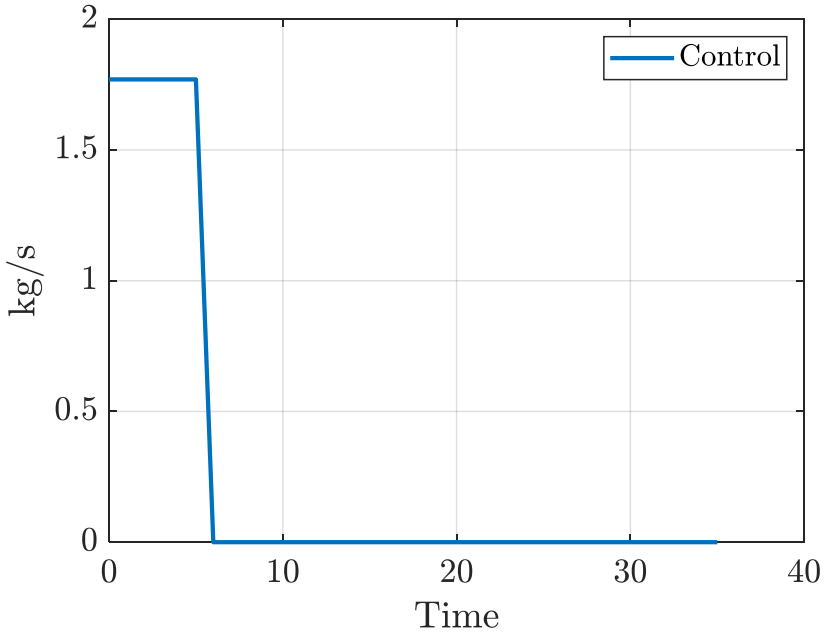

Figure 1. System Control Input

A. MEDIUM-FIDELITY MODEL

The first model developed from the truth model utilizes a varying drag coefficient and uses the NRLMSISE-00 atmospheric model. The drag coefficient for a rocket or other similar projectile must be experimentally determined. To develop the model, the estimated drag coefficient from Rocksim was used and is shown in Figure 2. The red line in the figure represents the total drag and the remaining lines depict the drag resulting from individual components.

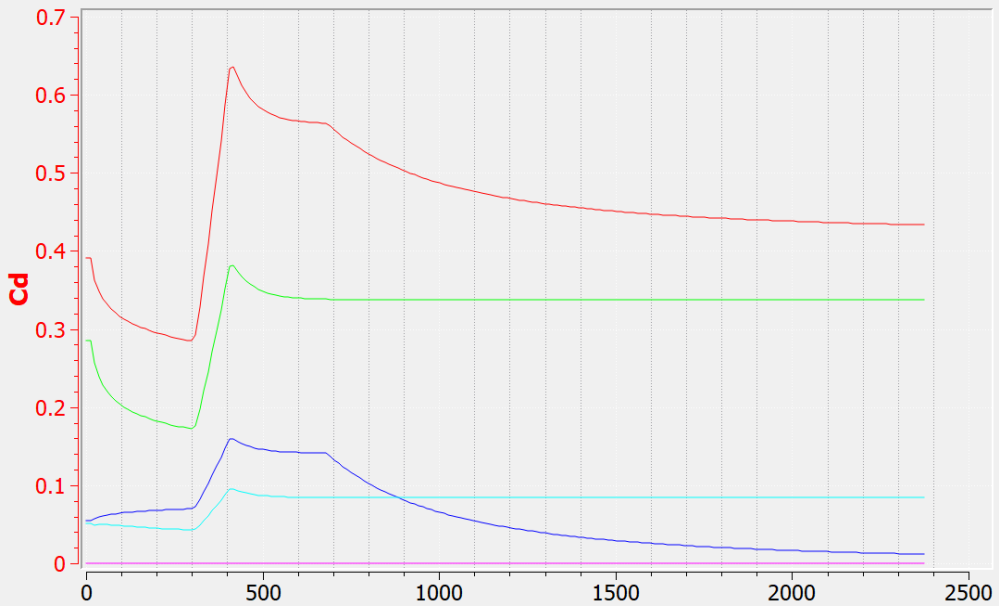

Figure 2. Drag Coefficient vs. Velocity (m/s). Source: [9].

The atmospheric density was modeled using the NRLMSISE-00 Atmosphere Model [10]. Using this model, the density at 100m increments was determined and linear interpolation was used to calculate the density at any altitude. This model captures the most up-to-date NASA atmospheric model and the highest-fidelity, drag-coefficient data that is obtainable without experimental testing of an actual system.

This first model was simulated, and the propagated states, altitude, velocity, and mass as well as the control for reference are as displayed in Figure 3.

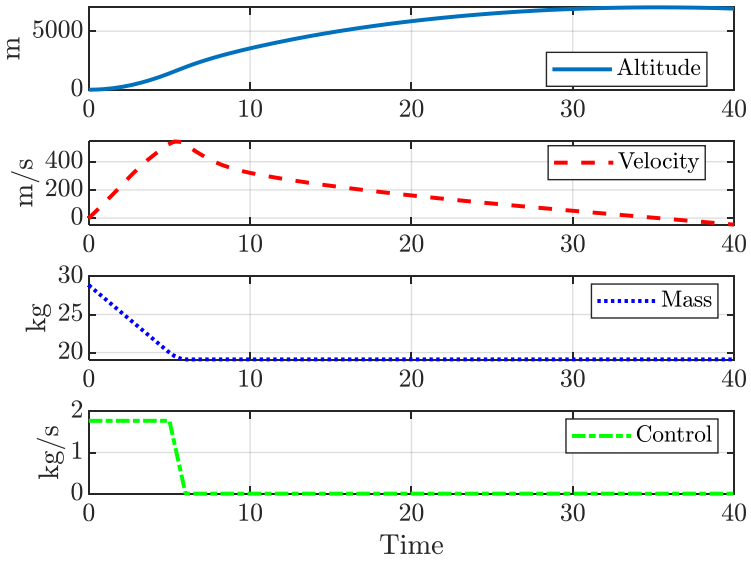

Figure 3. Medium-Fidelity Model Simulation

The simulated rocket in the medium fidelity model achieved an altitude of 7239 m with a max velocity of 568 m/s.

B. LOW-FIDELITY MODEL

The second model developed lowers the fidelity by utilizing a constant drag coefficient and an exponential atmospheric model. For this model, a drag coefficient of 0.5 was utilized because it was an average of the variable coefficient. The atmospheric density was modeled using an exponential decay model

$$\rho = \rho_0 e^{\frac{-r}{H}}$$

Where ρ_0 is the density at ground level and H is the scale height of the atmosphere (7,400 m). The states and control for this model are the same as the Medium-Fidelity model.

The Low-Fidelity Model was simulated, and the resulting states, altitude, velocity, and mass are shown in Figure 4.

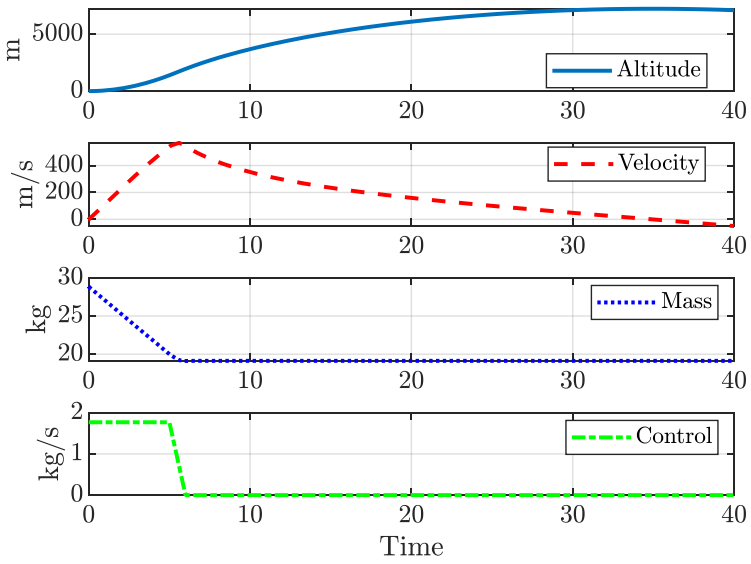

Figure 4. Low-Fidelity Model Simulation

Both the medium and low-fidelity models produced extremely similar results with a difference in maximum altitude of 94 m higher for the low-fidelity model and maximum velocity difference of 20 m/s. This difference is due to using a near average drag value and as shown in Figure 5 similar air densities profiles.

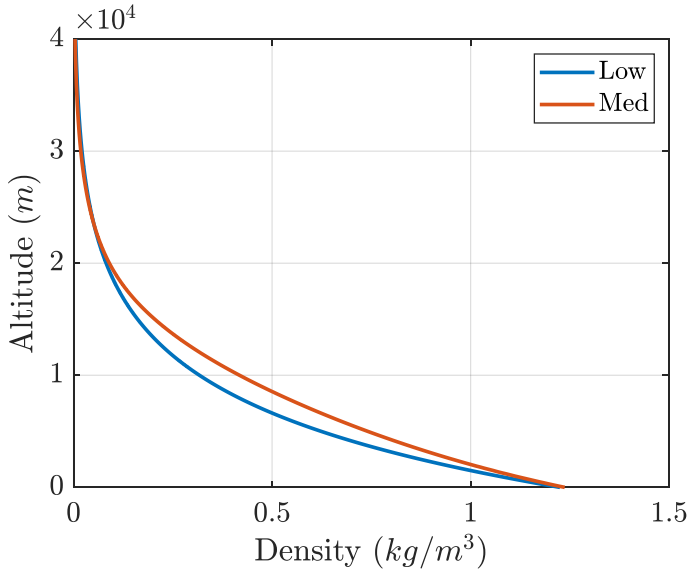

Figure 5. Air Density ve. Altitude by Model

C. ZERO-DRAG MODEL

The last model analyzed was a zero-drag model. For this model, the drag was assumed to be negligible and as a result the state equations simplify to

$$\dot{r} = v$$
$$\dot{v} = \frac{u \cdot c}{m} - \frac{\mu}{(r + \mathrm{R_e})^2}$$
$$\dot{m} = -u$$

Even though the equations changed the control for this model, a motor burning at maximum thrust for five seconds is the same as the previous two models. The zero-drag model was simulated to determine the difference with the previous models. As shown in Figure 6, the no-drag simulation resulted in higher altitude, speed and a longer time to apogee than the medium and low-fidelity models. At a time of 35 seconds the first two models had reached apogee. In comparison, the no-drag model achieved apogee at approximately 80 seconds at an altitude of over 28,000 meters.

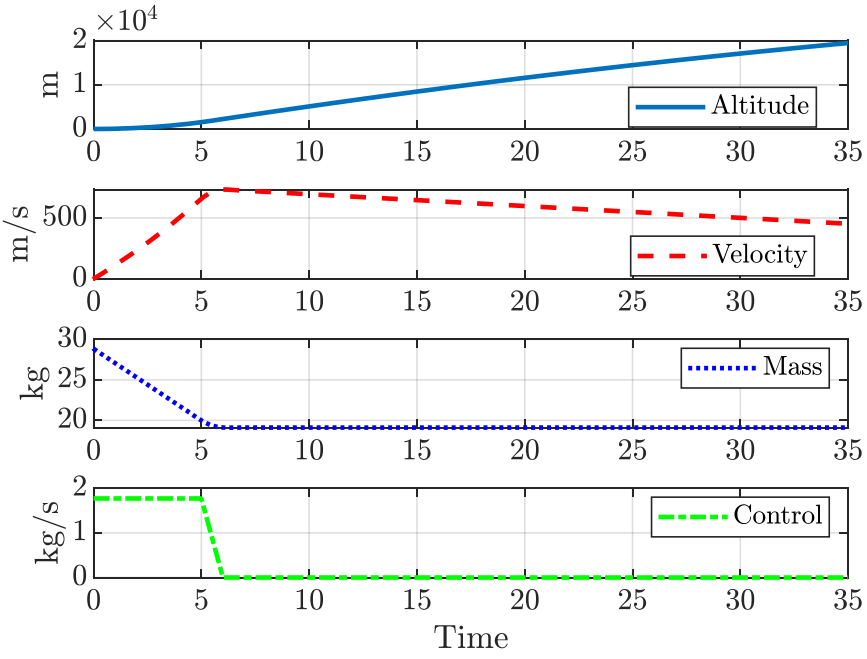

Figure 6. No-Drag Simulation

Given that the higher fidelity compared to the low-fidelity model resulted in a little more than one percent difference in altitude, the low-fidelity model was chosen to be used for the optimal control problem. The simplified model results in a less computationally expensive model to analyze. The NRLMSISE density model also relies on a table look-up and interpolation, thus introducing possible error and an inability to adequately apply the optimal control theories. All subsequent optimal control models relied solely on an exponential air density and constant drag model.

IV. SINGLE STAGE ALTITUDE OPTIMIZATION

The purpose of applying trajectory planning and optimal control theory to this project is to obtain a model that will be used to determine the maximum altitude that can be achieved given a specific propellant mass. It is important to determine this altitude in order to obtain a waiver to Federal Aviation Administration (FAA) or to remain within an existing waiver [5].

The rocket developed in [1] shown in Figure 7 was utilized as a starting reference.

Figure 7. CAD Rendering of Previous Design. Source: [1].

Following a failure during flight, modifications were made to eliminate the transitions between the nose cone and the booster stage to increase the durability of the design. Figure 8 displays the rocket design utilized for the analysis in this thesis. The first stage of the rocket is a 152 mm (six-inch) booster utilizing a commercial off the shelf (COTS) 150 mm rocket motor. The sustainer is also a 152 mm (six-inch) airframe and uses a COTS 98 mm motor. This allows the rocket to carry a 3U CubeSat in the nose cone.

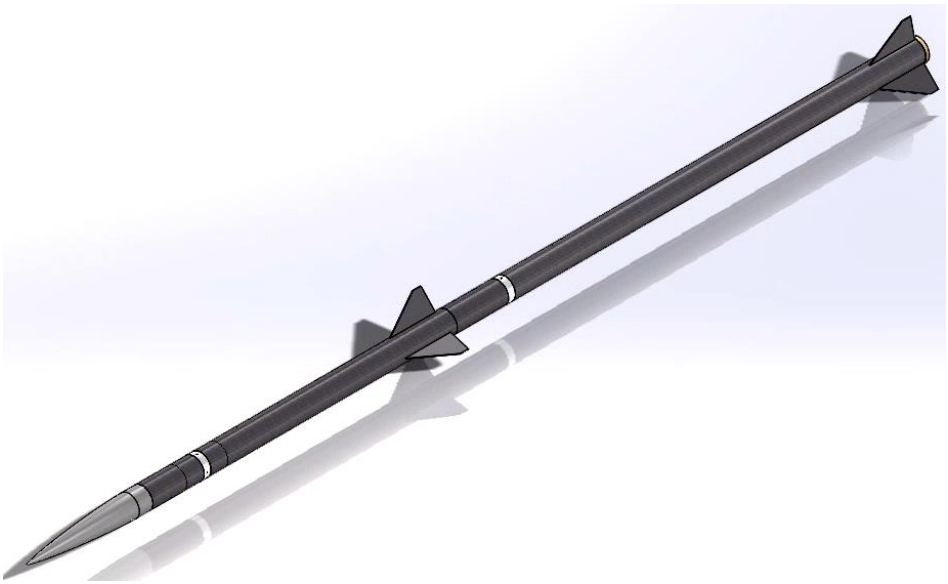

Figure 8. CAD Rendering of Two-Stage Rocket Design
Adapted from: [1]

This rocket utilizes COTS solid rocket motors; however, this research analyzes an optimally controlled (with respect to mass flow rate) rocket motor with a fixed exit velocity determined by the characteristic velocity of the motor. Because this thesis seeks to expand on the "Goddard Problem" of determining the maximum altitude of a one dimensional rocket [7], the control for this problem is the rate at which the mass is ejected from the rocket body. The problem was constrained by limiting the thrust acceleration to simulate a maximum acceleration of the rocket. This constraint could easily be changed to limit only the control, mass flow rate, or any other state variable and control combination. This problem will map to a theoretical maximum altitude that could be achieved using the propellant mass of the given rocket motor while setting a maximum acceleration. Two models were utilized, a zero-drag model and a higher fidelity model with drag. The zero-drag model is useful in verifying the thrust and gravity terms of the higher fidelity model as well as verifying the code utilized. The second was a dynamical model that used a constant drag coefficient and a simple exponential model for atmospheric density.

The dynamics for this specific problem are as follows:

$$
\begin{cases}
\textit{State}: & \mathbf{x} := (x, v, m) & \\
\textit{Control}: & \mathbf{u} := u & \\
\textit{Maximize} & J[\underline{x}(\cdot), \underline{u}(\cdot), t_f] & = r(t_f) \\
\textit{Subject to} & \dot{r} & = v \\
 & \dot{v} & = \dfrac{u \cdot c}{m} - \dfrac{\rho(r)}{2m} C_D A v^2 - \dfrac{\mu_g}{(r + \mathrm{Re})^2} \\
 & \dot{m} & = -u \\
 & (r_0, v_0, m_0, t_0) & = (0, 0, M_0, 0) \\
 & e_1(\underline{x}_f) & := m_f - M_f \\
 & h_1 & 0 \le \dfrac{u \cdot c}{m} \le a_{\max}
\end{cases}
$$

For this problem the parameters were defined utilizing the proposed rocket body with the expected commercial motor characteristics [11] as shown in Table 1.

Table 1. Single-Stage Constant Values

Constant	Value
a_{Max}	150 [m/s^2]
R_e	6,378,000 [m]
M_0	28.84 [kg]
M_f	17.91 [kg]
c	1927.67 [m/s]
C_D	0.4
A	0. 018241 [m^2]
H	7400 [m]
ρ	1.225 [kg/m^3]
μ_g	3.968x10^{14} [m^3/s^2]

Employing a six-inch rocket body diameter and Von Kármán nose cone specifies the area, drag coefficient, and dry mass of the rocket including the payload. For this analysis the payload was assumed to have a fixed mass carried to apogee. While varying this mass would affect the overall achievable altitude its mass relative to the mass of the rocket is small. Using the data for the O3400 rocket motor, the propellant mass, motor dry mass, and exit velocity were determined. The acceleration limit was set at approximately 15 g because this resulted in a maximum mass flow rate equivalent to the O3400 motor. Exit velocity, *c*, was established by utilizing the I_{sp} of the rocket motor. The remaining

constants were based on given earth parameters. DIDO was chosen to solve the problem due to the long time-horizon and the expected bang-bang type controller. Based on previous class work, DIDO works best for these style problems. All the appropriate functions required for DIDO to run properly were developed in MATLAB.

A. SCALING AND PONTRYAGIN'S PRINCIPLE

1. Scaling

Due to the vast difference in the values of r, v, and m, scaling was required for this problem. DIDO was unable to achieve a solution without scaling at a minimum the r and v states. Designer scaling units are used because they allow each state to be scaled independently of the other states. By comparison canonical scaling keeps the mathematical relationships normally held such as velocity is equal to length divided time. When using designer units these relationships do not necessarily hold [12]. These scaling units were used in order to better balance the individual state/costate pairs.

$$\tilde{r} = \frac{r}{L}, \tilde{v} = \frac{v}{V}, \tilde{m} = \frac{m}{M}, \tilde{u} = \frac{u}{U} \tag{4.1}$$

The following scaling factors were chosen via trial and error to keep the relative magnitudes of the state/costate pairs balanced and are shown in Table 2.

Table 2. Single Stage Scaling Factors

Scale	Value
L	4500
V	300
M	10
T	1
u	1

Using designer scaling units allows the dynamics equations to be propagated in engineering units and then be multiplied by a scaling factor to scale the entire equation. The next step of scaling the problem was to scale the dynamics equations.

$$\frac{d\tilde{r}}{d\tilde{t}} = \frac{d(r/L)}{d(t/T)} = \frac{dr}{dt}\frac{T}{L} = \frac{T}{L}v$$

$$\frac{d\tilde{v}}{d\tilde{t}} = \frac{d(v/V)}{d(t/T)} = \frac{dv}{dt}\frac{T}{V} = \frac{T}{V}\left[\frac{u\cdot c}{m} - \frac{1}{2m}C_D A v^2 \rho(r) - \frac{\mu_g}{(r+\mathrm{Re})^2}\right]$$

$$\frac{d\tilde{m}}{d\tilde{t}} = \frac{d(m/M)}{d(t/T)} = \frac{dm}{dt}\frac{T}{M} = -\frac{T}{M}u \tag{4.2}$$

This derivation yields the following dynamics:

$$\underline{\tilde{x}} = \begin{bmatrix} \tilde{r} \\ \tilde{v} \\ \tilde{m} \end{bmatrix}, \underline{\dot{\tilde{x}}} = \begin{bmatrix} \frac{T}{L}v \\ \frac{T}{V}\left[\frac{u\cdot c}{m} - \frac{1}{2m}C_D A v^2 \rho(r) - \frac{\mu_g}{(r+\mathrm{Re})^2}\right] \\ -\frac{T}{M}u \end{bmatrix}, u = \begin{bmatrix} u \\ U \end{bmatrix} \tag{4.3}$$

2. Pontryagin's Principle

Applying Pontryagin's Principle to the OCP, the "HAMVET" process must be applied. The first step in "HAMVET" is to develop the Hamiltonian.

$$H = F + \lambda^T f(x,u)$$
$$H = 0 + \lambda_r v + \lambda_v\left[\frac{u\cdot c}{m} - \frac{\rho(r)}{2m}C_D A v^2 - \frac{\mu_g}{(r+\mathrm{Re})^2}\right] + \lambda_m(-u) \tag{4.4}$$

Then the Lagrangian of the Hamiltonian is developed:

$$\bar{H}(\mu,\lambda,x,u,t) = H(\lambda,x,u,t) + \mu^T u$$
$$\bar{H} = H + \mu^T u \tag{4.5}$$
$$\bar{H} = \lambda_r v + \lambda_v\left[\frac{u\cdot c}{m} - \frac{\rho(r)}{2m}C_D A v^2 - \frac{\mu_g}{(r+\mathrm{Re})^2}\right] + \lambda_m(-u) + \mu^T\frac{u\cdot c}{m}$$

Next the Hamiltonian Minimization Condition (HMC) is determined:

$$HMC = \begin{cases} Minimize & H(\lambda, x, u, t) \\ Subject & h^L \le h(u) \le h^U \end{cases}$$

$$\frac{\partial \bar{H}}{\partial u} = \frac{\partial H}{\partial u} + \left(\frac{\partial h}{\partial u}\right)^T \mu = 0 = \frac{\lambda_v \cdot c}{m} - \lambda_m + \mu \frac{c}{m} \tag{4.6}$$

$$\mu = \frac{\lambda_m \cdot m}{c} - \lambda_v$$

Based on the Karush-Kuhn-Tucker (KKT) Complementarity conditions, the control is as follows:

$$\mu = \begin{cases} \le 0 & if \quad h(x,u) = h^L \\ 0 & if \quad h^L < h(x,u) < h^U \\ \ge 0 & if \quad h(x,u) = h^U \end{cases} \tag{4.7}$$

The next step is to apply the adjoint equations:

$$\frac{\delta H}{\delta \underline{x}} = -\dot{\underline{\lambda}}$$

$$\frac{\delta H}{\delta r} = -\dot{\lambda}_r = \lambda_v \left[\frac{\dot{\rho}(r)}{2m} C_D A v^2 - \frac{2\mu}{(r + \mathrm{Re})^3} \right] \Rightarrow \dot{\lambda}_r = \lambda_v \left[-\frac{\dot{\rho}}{2m} C_D A v^2 + \frac{2\mu}{(r + \mathrm{Re})^3} \right],$$

$$\frac{\delta H}{\delta v} = -\dot{\lambda}_v = \lambda_r - \lambda_v \frac{\rho}{m} C_D A v \Rightarrow \dot{\lambda}_v = \lambda_v \frac{\rho}{m} C_D A v - \lambda_r$$

$$\frac{\delta H}{\delta m} = -\dot{\lambda}_m = \lambda_v \left[-\frac{u \cdot c}{m^2} + \frac{\rho}{2m^2} C_D A v^2 \right] - \mu \frac{u \cdot c}{m^2} \Rightarrow \dot{\lambda}_m = \lambda_v \left[\frac{u \cdot c}{m^2} - \frac{\rho}{2m^2} C_D A v^2 \right] + \mu \frac{u \cdot c}{m^2}$$

(4.8)

For this problem, six boundary conditions are required to solve the system, and four are given in the problem statement; thus, the state/costate transversality equations will yield the remaining two boundary conditions.

$$
\begin{aligned}
&\bar{E} = E + \nu^T e \\
&\bar{E} = -r_f + \nu_x (m_f - M_f) \\
&\frac{\delta \bar{E}}{\delta \underline{x}_f} = \underline{\lambda}(t_f) \\
&\frac{\delta \bar{E}}{\delta r_f} = \lambda_r(t_f) = -1 \\
&\frac{\delta \bar{E}}{\delta v_f} = \lambda_v(t_f) = 0 \\
&\frac{\delta \bar{E}}{\delta m_f} = \lambda_m(t_f) = \nu
\end{aligned}
\tag{4.9}
$$

The next step is to find the optimal stopping condition by analyzing the Hamiltonian value condition (HVC).

$$
\begin{aligned}
&H\left[@t_f\right] = -\frac{\delta \bar{E}}{\delta t_f} \\
&\frac{\delta \bar{E}}{\delta t_f} = 0 \Rightarrow H\left[@t_f\right] = 0
\end{aligned}
\tag{4.10}
$$

The last step to applying the "HAMVET" process is to evaluate the Hamiltonian Evolution Equation (HEE). This equation proves that the minimized Hamiltonian evolves according to the formula:

$$
\begin{aligned}
&\frac{d\mathrm{H}}{dt} = \frac{\delta H}{\delta t} \\
&\frac{\delta H}{\delta t} = 0 \Rightarrow \frac{d\mathrm{H}}{dt} = 0
\end{aligned}
\tag{4.11}
$$

According to the last two equations the value of the Hamiltonian is constant with respect to time and equal to 0.

3. V&V Equations

The important equations for validation and verification (V&V) are the dynamics of all three costates should not be linear and non-zero. Transversality equations determined

that λ_r and λ_v costates should end at -1 and 0 respectively. The control will be determined by the KKT Complementarity conditions. This in conjunction with the constancy of the Hamiltonian will prove the optimality of the system.

Using the system dynamics and the derived control

$$\begin{aligned}\dot{r} &= v \\ \dot{v} &= \frac{u \cdot c}{m} - \frac{\rho(r)}{2m} C_D A v^2 - \frac{\mu}{(r+\mathrm{Re})^2} \\ \dot{m} &= -u\end{aligned} \tag{4.12}$$

The system state dynamics can be propagated using ode45 to determine the feasibility of the optimal control.

B. RESULTS ANALYSIS

The two separate models were analyzed, a low-fidelity, no-drag model and a medium fidelity constant drag model with an exponential atmospheric density profile. Both models were constrained using an arbitrary 150 m/s^2 thrust acceleration limit.

1. No-Drag Model

For the first model, drag was neglected, resulting in a simplified dynamics model. This model was run using 25 nodes. The only difference in the application of Pontryagin's Principle is the adjoint equations change as follows:

$$\begin{aligned}\frac{\delta H}{\delta r} &= -\dot{\lambda}_r = \lambda_v \left[-\frac{2\mu}{(r+\mathrm{Re})^3} \right] \Rightarrow \dot{\lambda}_r = \frac{2\lambda_v \mu}{(r+\mathrm{Re})^3} \\ \frac{\delta H}{\delta v} &= -\dot{\lambda}_v = \lambda_r \Rightarrow \dot{\lambda}_v = -\lambda_r \\ \frac{\delta H}{\delta m} &= -\dot{\lambda}_m = -\frac{\lambda_v u \cdot c}{m^2} - \mu \frac{\lambda_v u \cdot c}{m^2} \Rightarrow \dot{\lambda}_m = \frac{\lambda_v u \cdot c}{m^2} + \mu \frac{\lambda_v u \cdot c}{m^2}\end{aligned} \tag{4.13}$$

All the remaining necessary conditions are unchanged. The first step is to test the optimality of the system. Figures 9 and 10 show the DIDO output for the states and control as a function of time for scaled and unscaled units, respectively.

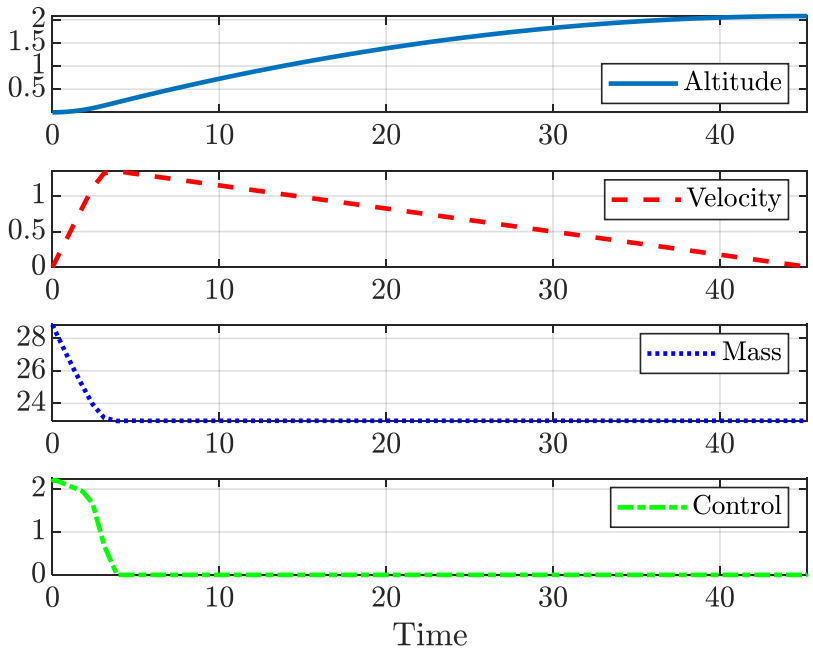

Figure 9. No-Drag Scaled States and Control

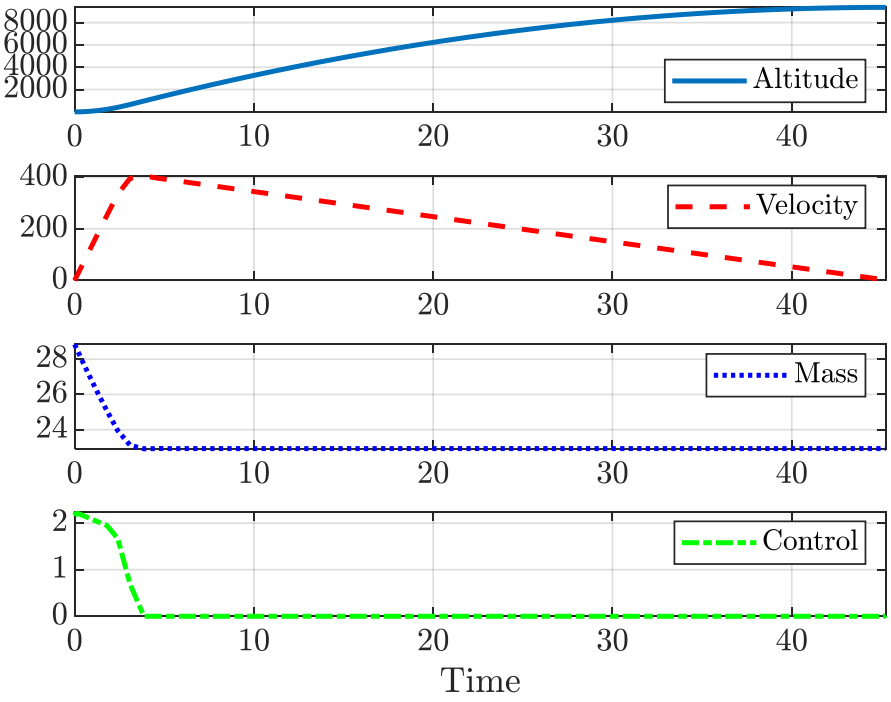

Figure 10. No-Drag Unscaled States and Control

The next step is to test the optimality by examining the behavior of the costates. The adjoint equations state the slope of λ_v is equal to the negative of λ_r , and since λ_r is nearly constant, λ_v is almost linear. λ_r ends at -1 and λ_v end at 0, meeting the transversality conditions. Figure 11 illustrates both conditions.

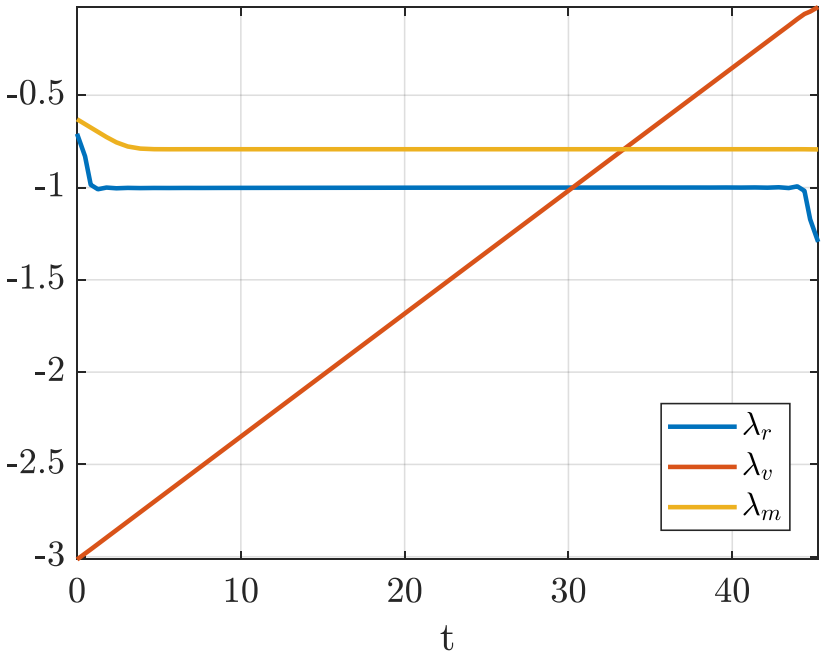

Figure 11. No-Drag Scaled Costates vs. Time

Next the constancy of the Hamiltonian and the Hamiltonian endpoint condition behaves according to the HVC and HEE. Figure 12 depicts the Hamiltonian is nearly constant apart from during the thrust portion of flight. This constant value is partly due to the limited number of nodes used to achieve a balance between the constancy of the Hamiltonian and the endpoints of the adjoint equations.

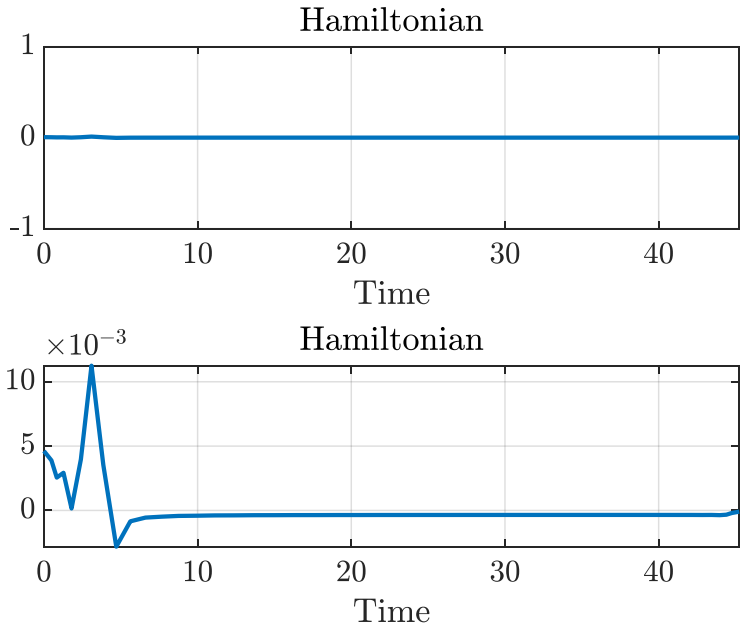

Figure 12. Hamiltonian vs. Time

For this problem, stationarity was analyzed, this produced an interesting result. During the thrust portion of the flight, the stationarity condition is nearly zero, however, when the control is no longer active the condition no longer holds.

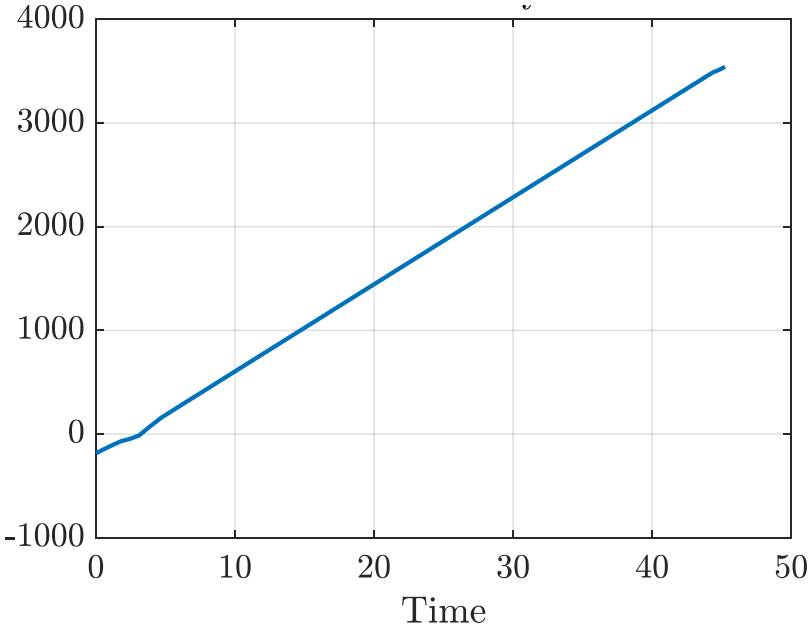

Figure 13. No-Drag Stationarity Condition

The last step to test the optimality of the system is to observe that the control behaves in accordance with the Complementarity conditions. Figure 14 shows that the control is at the upper bound when μ is positive. Since the state constraint only applies to the thrust acceleration after motor burnout, the thrust acceleration is zero making the μ zero.

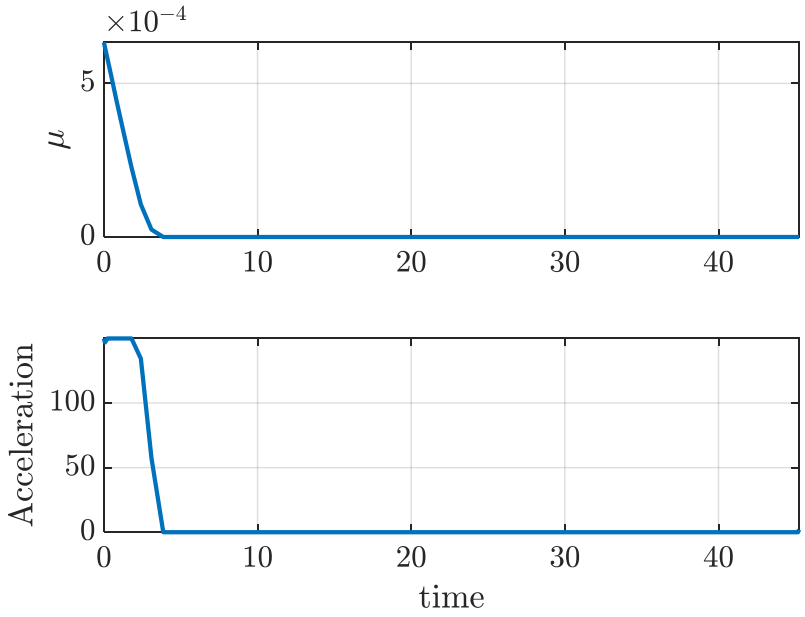

Figure 14. Complementarity Conditions

Next, the feasibility was tested by using the control obtained from DIDO to propagate the plant dynamics. Figure 15 shows the propagated states using the optimal control as they compare to the state outputs from DIDO.

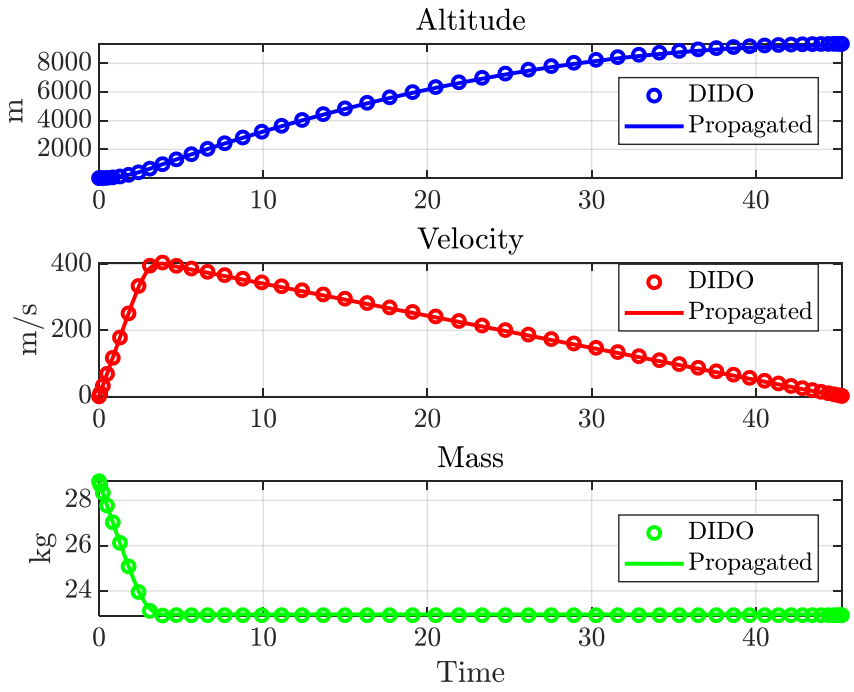

Figure 15. Feasibility Test

The above tests prove that the controller is both extremal and feasible.

2. Medium-Fidelity Model

Next, the medium fidelity drag model was used to determine the optimal control trajectory. For this model, 50 nodes were used. The first step is to test the optimality of the system. Figures 16 and 17 show the DIDO output for the states and control as a function of time for scaled and unscaled units, respectively.

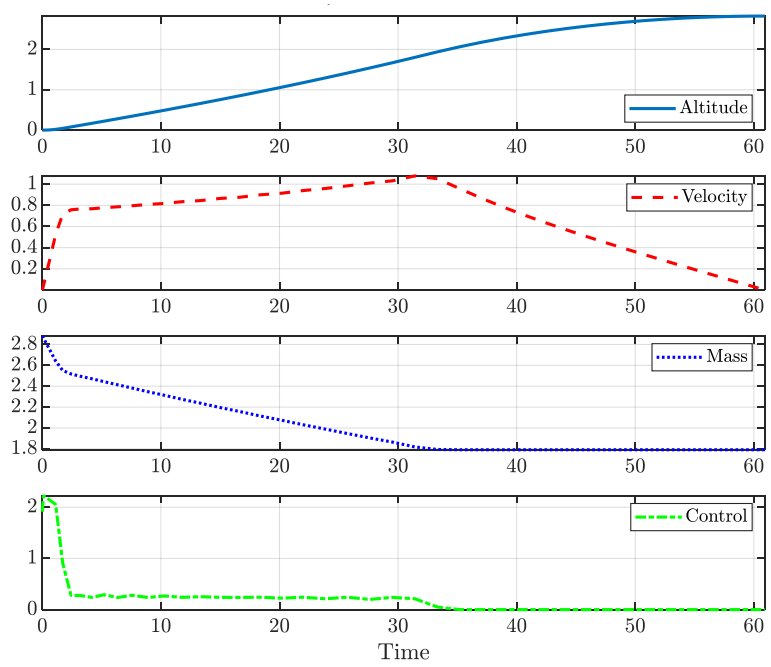

Figure 16. Scaled States and Control

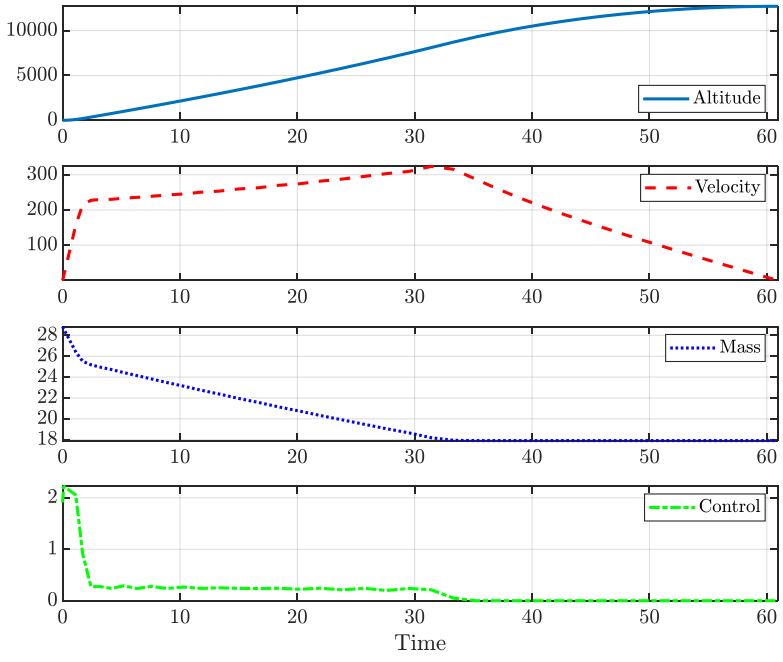

Figure 17. Unscaled States and Control

The optimally controlled single stage rocket achieved an altitude of 12.7 km mean sea level (MSL) (41000 ft). The next step is to test the optimality by examining the behavior of the costates. As established in the "HAMVET" process, the costates should not be linear or constant as well as λ_r ending at -1 and λ_v ending at 0 as illustrated in Figure 18.

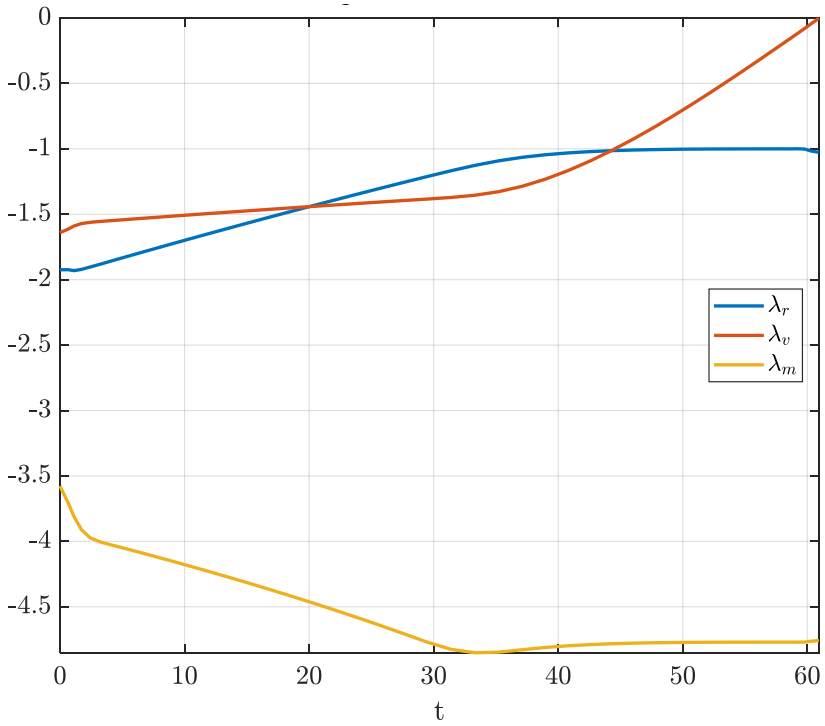

Figure 18. Costates vs. Time

Next, the constancy of the Hamiltonian and the Hamiltonian endpoint condition behaves according to the HVC and HEE. Figure 19 depicts the Hamiltonian is nearly constant as a function of time with slight transients at the beginning where control is changing during the thrust portion of flight.

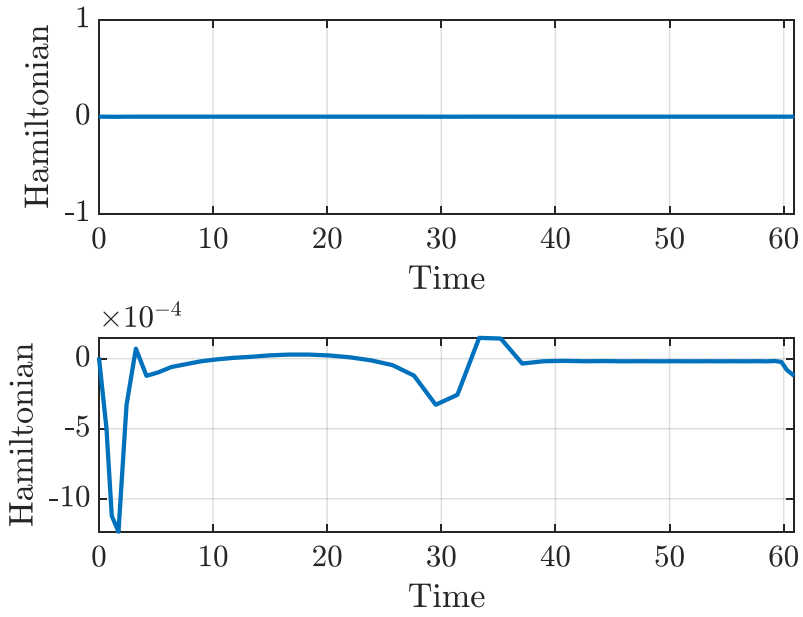

Figure 19. Hamiltonian vs. Time

Similar to the no-drag case, Figure 20 illustrates that the stationarity condition held for the portion of the flight where the control was active but following this portion the stationarity fails.

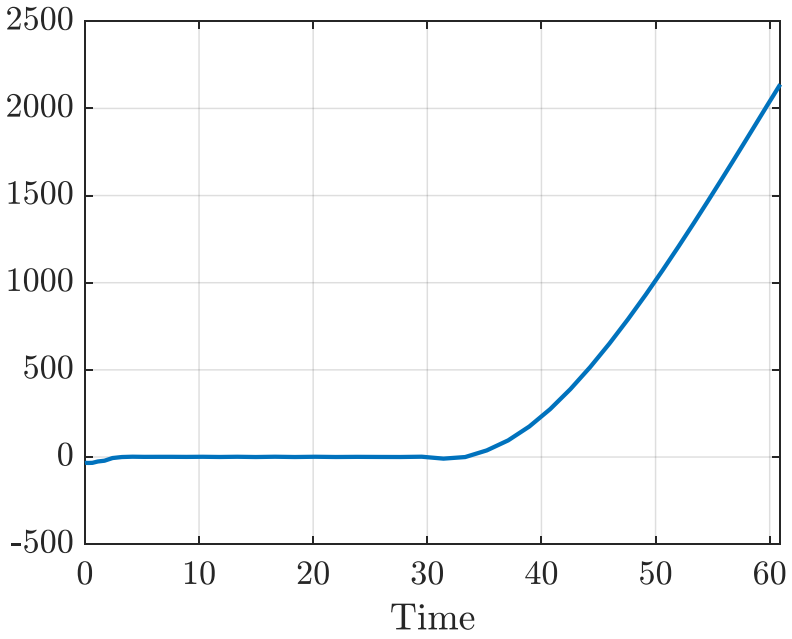

Figure 20. Stationarity Condition

The last step to test the optimality of the system is to observe that the control behaves in accordance with the KKT Complementarity conditions. Figure 21 proves that the system behaves according to the KKT Complementarity conditions.

$$\mu = \begin{cases} \leq 0 & if \quad h(u) = h^L \\ 0 & if \quad h^L < h(u) < h^U \\ \geq 0 & if \quad h(u) = h^U \end{cases}$$

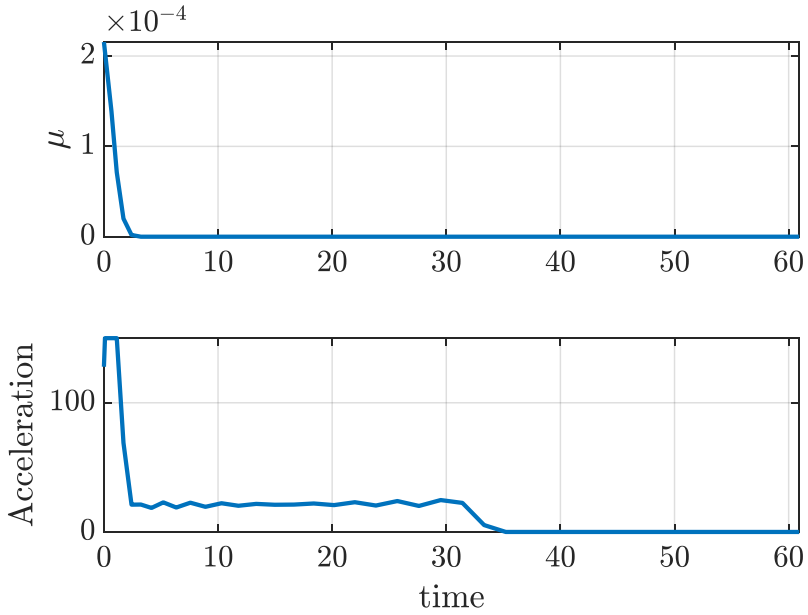

Figure 21. Complementarity Conditions

Next, the feasibility was tested by using the control obtained from DIDO to propagate the plant dynamics. Figure 22 shows the propagated states using the optimal control as they compare to the state outputs from DIDO.

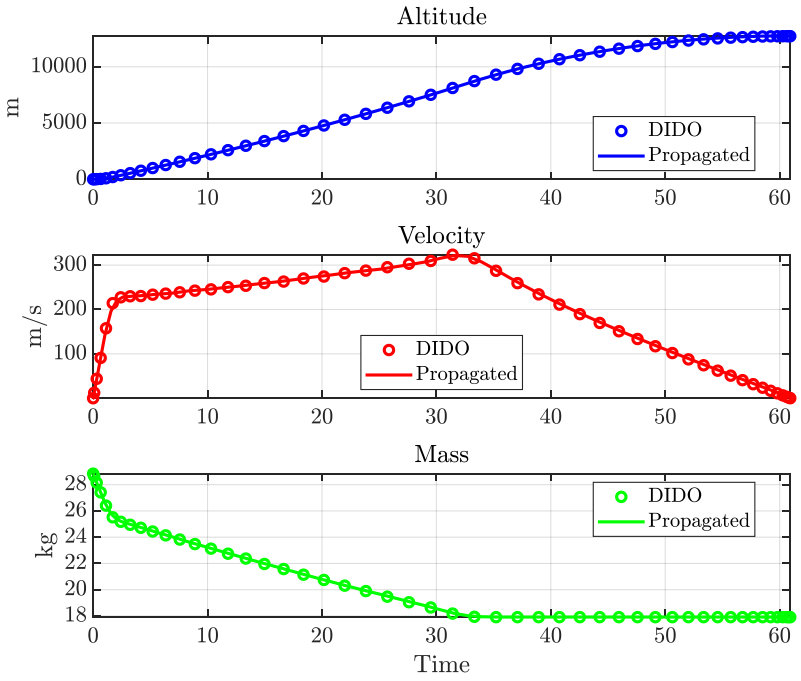

Figure 22. Feasibility Test

One major difference between both models is that the low-fidelity model expends all its fuel in the quickest amount of time to achieve the greatest speed possible. The drag model however throttles the engine in order to limit the amount of parasitic drag on the system. While similar results could be achieved using a bang-bang style control, the throttled control achieved a 3.5 km higher altitude. Figure 23 shows that while the bang-bang controlled rocket achieves a higher velocity the drag causes the velocity of the bang-bang control to decrease quicker than the optimal control.

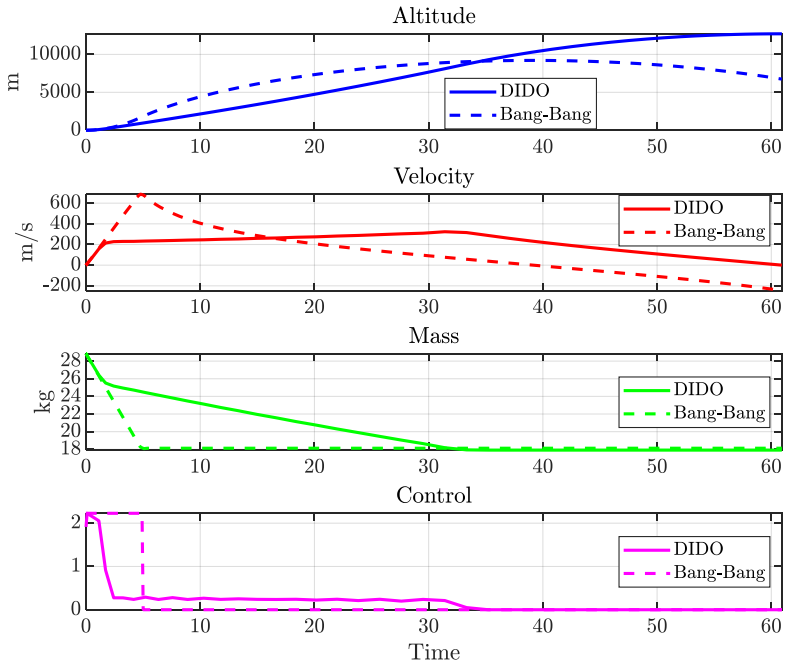

Figure 23. Bang-Bang vs. Optimal Control

While the optimal control trajectory can achieve a higher altitude, there would be a significant increase in complexity to develop and field a rocket motor utilizing the optimal control trajectory. To achieve this varying mass flow rate a liquid rocket motor would have to be utilized. Similar to the bang-bang control, Figure 24 compares the commercially available O3400 motor to the optimal control model. Using the thrust profile of the O3400 motor and the calculated exit velocity the mass flow rate was determined.

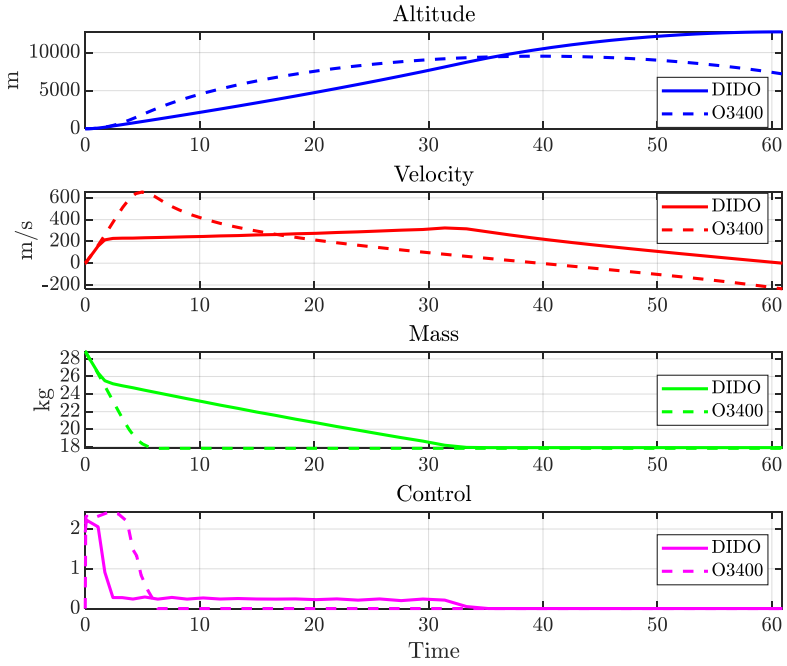

Figure 24. Optimal Control vs. O3400 Motor

This COTS motor simulation was then compared to the bang-bang controller. The mass flow rate as determined by the thrust profile for a COTS motor can be closely approximated by the bang-bang style controller as shown in Figure 25.

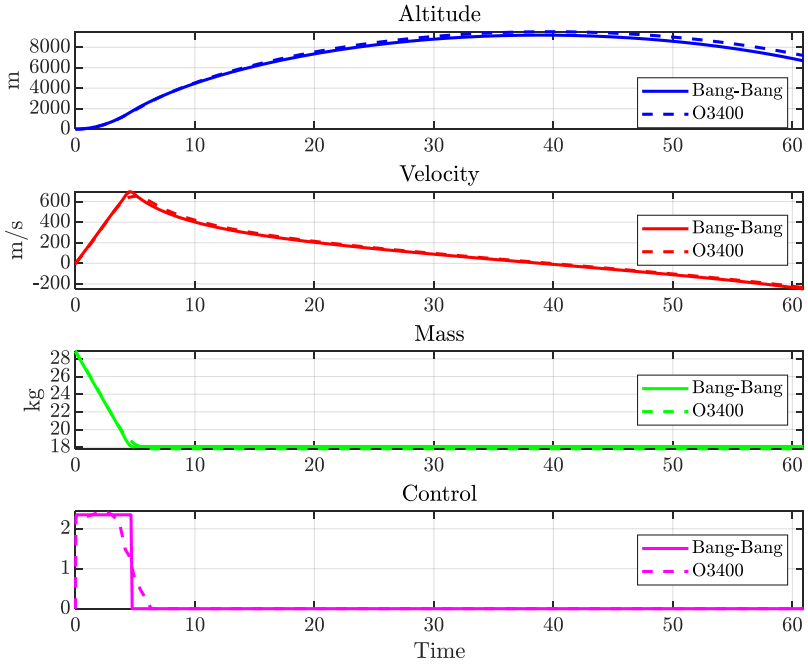

Figure 25. Bang-Bang vs. O3400 Motor

There is a difference of 333 meters in apogee altitude and a max difference of 23 meters per second velocity. This comparison shows that the bang-bang style controller can be utilized to approximate the COTS motor for two-stage simulation development.

THIS PAGE INTENTIONALLY LEFT BLANK

V. TWO-STAGE ROCKET DEVELOPMENT

Following determining the model for a one stage rocket, the was then expanded to a two-stage, rocket. To adequately solve a multistage rocket problem, the state space must be expanded to separate each stage into two phases, a boost phase, and a coast phase. The boost phase is defined as the time during which the motor is thrusting and the coast phase is defined as the time when the rocket is flying without motor thrust following motor burn out. The rocket is assumed to stage the first stage booster using the ignition of the second stage motor to provide the separation mechanism. This means that the discontinuity resulting from the stage separation is collocated with the ignition of the second stage motor. Each phase consists of the same dynamics utilized for solving the single stage rocket problem. The state space dynamics and optimal control problem are as follows:

$$
\begin{cases}
\textit{State}: & \mathbf{x} := (r_1, v_1, m_1, r_2, v_2, m_2, r_3, v_3, m_3, r_4, v_4, m_4) \\
\textit{Control}: & \mathbf{u} := (u_1, u_2, u_3, u_4) \\
\textit{Maximize} & J[\underline{x}(\cdot), \underline{u}(\cdot), t_f] = r_4(t_f) \\
\textit{Subject to} & \dot{r}_1 = v_1 p_1 \\
& \dot{v}_1 = \left[\frac{u_1 \cdot c}{m_1} - \frac{\rho(r_1)}{2m_1} C_D A v_1^2 - \frac{\mu_g}{(r_1 + \mathrm{Re})^2} \right] p_1 \\
& \dot{m}_1 = -u_1 p_1 \\
& \dot{r}_2 = v_2 p_2 \\
& \dot{v}_2 = \left[\frac{u_2 \cdot c}{m_2} - \frac{\rho(r_2)}{2m_2} C_D A v_2^2 - \frac{\mu_g}{(r_2 + \mathrm{Re})^2} \right] p_2 \\
& \dot{m}_2 = -u_2 p_2 \\
& \dot{r}_3 = v_3 p_3 \\
& \dot{v}_3 = \left[\frac{u_3 \cdot c}{m_3} - \frac{\rho(r_3)}{2m_3} C_D A v_3^2 - \frac{\mu_g}{(r_3 + \mathrm{Re})^2} \right] p_3 \\
& \dot{m}_3 = -u_3 p_3 \\
& \dot{r}_4 = v_4 p_4 \\
& \dot{v}_4 = \left[\frac{u_4 \cdot c}{m_4} - \frac{\rho(r_4)}{2m_4} C_D A v_4^2 - \frac{\mu_g}{(r_4 + \mathrm{Re})^2} \right] p_4 \\
& \dot{m}_4 = -u_4 p_4 \\
& (r_{1,0}, v_{1,0}, m_{1,0}, t_0) = (0, 0, M_0, 0) \\
& (r_{2,0}, v_{2,0}, m_{2,0}) = (r_{1,f}, v_{1,f}, m_{1,f}) \\
& (r_{3,0}, v_{3,0}, m_{3,0}) = (r_{2,f}, v_{2,f}, m_{2,f} - M_{stage}) \\
& (r_{4,0}, v_{4,0}, m_{4,0}) = (r_{3,f}, v_{3,f}, m_{3,f}) \\
& e_1(\underline{x}_f) = m_{2,f} - M_1^f \\
& e_2(\underline{x}_f) = m_{4,f} - M_2^f \\
& h \qquad u_{\min} \le u \le u_{\max}
\end{cases}
$$

For this problem, M_1^f and M_2^f represent the dry weight of at burnout for each stage. M_0 and M_{stage} represent the initial weight with loaded motors and the weight to be staged, respectively. For these dynamics, p_1 through p_4 are parameters that allow the dynamics to be run on a fixed time interval 0 to 1. The optimal control solver then determines the correct value for these parameters to determine the exact timing of each phase. The phase endpoint

constraints work to "stitch" the phases together by forcing the phase to start at the endpoint of the previous stage. The only exception is the mass from phase 2 to 3 which has the staging mass discontinuity.

For this problem, the parameters were defined utilizing the proposed rocket body with the expected commercial motor characteristics. This rocket is expected to utilize a Q8955 motor for the first stage booster and a O3400 for the second stage sustainer [11], [13]. Table 3 defines the constant values for the optimal control problem such as, drag coefficient, the various masses, exit velocities, and global constants.

Table 3. Constant Values

Constant	Value
R_e	6,378,000 [m]
M_0	98.68 [kg]
$M_{1,f}$	57.93 [kg]
M_{stage}	24.09 [kg]
$M_{2,f}$	22.91 [kg]
c_1	2297.4 [m/s]
c_2	1927.7 [m/s]
C_D	0.5
A	0. 018241 [m^2]
H	7400 [m]
ρ	1.225 [kg/m^3]
μ_g	$3.968x10^{14}$ [m^3/s^2]

Once the OCP is developed, Scaling and Pontryagin's principle can be applied.

A. PONTRYAGIN'S PRINCIPLE

The steps remain the same for this expanded problem. The first step to applying Pontryagin's Principle is to develop the Hamiltonian and the Lagrangian of the Hamiltonian:

$$H(\lambda,x,u,t)=F+\lambda^T f(x,u)$$

$$H=\begin{array}{l}0+\lambda_{r_1}v_1+\lambda_{v_1}\left[\dfrac{u_1\cdot c_1}{m_1}-\dfrac{\rho(r_1)}{2m_1}C_D A{v_1}^2-\dfrac{\mu_g}{(r_1+\mathrm{Re})^2}\right]+\lambda_{m_1}(-u_1)\ldots\\ \lambda_{r_2}v_2+\lambda_{v_2}\left[\dfrac{u_2\cdot c_1}{m_2}-\dfrac{\rho(r_2)}{2m_2}C_D A{v_2}^2-\dfrac{\mu_g}{(r_2+\mathrm{Re})^2}\right]+\lambda_{m_2}(-u_2)\ldots\\ \lambda_{r_3}v_3+\lambda_{v_3}\left[\dfrac{u_3\cdot c_2}{m_3}-\dfrac{\rho(r_3)}{2m_3}C_D A{v_3}^2-\dfrac{\mu_g}{(r_3+\mathrm{Re})^2}\right]+\lambda_{m_3}(-u_3)\ldots\\ \lambda_{r4}v_4+\lambda_{v_4}\left[\dfrac{u_4\cdot c_2}{m_4}-\dfrac{\rho(r_4)}{2m_4}C_D A{v_4}^2-\dfrac{\mu_g}{(r_4+\mathrm{Re})^2}\right]+\lambda_{m_4}(-u_4)\end{array} \tag{5.1}$$

$$\bar{H}(\mu,\lambda,x,u,t)=H(\lambda,x,u,t)+\mu^T u$$

$$\bar{H}=\begin{array}{l}0+\lambda_{r_1}v_1+\lambda_{v_1}\left[\dfrac{u_1\cdot c_1}{m_1}-\dfrac{\rho(r_1)}{2m_1}C_D A{v_1}^2-\dfrac{\mu_g}{(r_1+\mathrm{Re})^2}\right]+\lambda_{m_1}(-u_1)\ldots\\ \lambda_{r_2}v_2+\lambda_{v_2}\left[\dfrac{u_2\cdot c_1}{m_2}-\dfrac{\rho(r_2)}{2m_2}C_D A{v_2}^2-\dfrac{\mu_g}{(r_2+\mathrm{Re})^2}\right]+\lambda_{m_2}(-u_2)\ldots\\ \lambda_{r_3}v_3+\lambda_{v_3}\left[\dfrac{u_3\cdot c_2}{m_3}-\dfrac{\rho(r_3)}{2m_3}C_D A{v_3}^2-\dfrac{\mu_g}{(r_3+\mathrm{Re})^2}\right]+\lambda_{m_3}(-u_3)\ldots\\ \lambda_{r4}v_4+\lambda_{v_4}\left[\dfrac{u_4\cdot c_2}{m_4}-\dfrac{\rho(r_4)}{2m_4}C_D A{v_4}^2-\dfrac{\mu_g}{(r_4+\mathrm{Re})^2}\right]+\lambda_{m_4}(-u_4)\ldots\\ +\mu_1u_1+\mu_2u_2+\mu_3u_3+\mu_4u_4\end{array} \tag{5.2}$$

The HMC is applied to the Lagrangian of the Hamiltonian for each control to determine its respective Lagrangian multiplier:

$$\begin{aligned}&HMC=\begin{cases}Minimize & H(\lambda,x,u,t)\\ Subject & h^L\le h(u)\le h^U\end{cases}\\ &\frac{\partial\bar{H}}{\partial u}=\frac{\partial H}{\partial u}+\left(\frac{\partial h}{\partial u}\right)^T\mu=0=\frac{\lambda_v\cdot c}{m}-\lambda_m+\mu\\ &\mu=\lambda_m-\frac{\lambda_v\cdot c}{m}\end{aligned} \tag{5.3}$$

The proper control is then determined using the KKT Complementarity conditions:

$$\mu = \begin{cases} \leq 0 & if \quad h(x,u) = h^L \\ 0 & if \quad h^L < h(x,u) < h^U \\ \geq 0 & if \quad h(x,u) = h^U \end{cases} \tag{5.4}$$

Next, the adjoint equations are applied to determine the dynamics of the costates. Each of the phase dynamics yields the same adjoint equations with the respective phase states, i.e. $\dot{\lambda}_{r_1} = f(r_1, v_1, m_1, \lambda_{r_1}, \lambda_{v_1}, \lambda_{m_1})$, thus each phase's costate state dynamics is a function of only the respective phase states and costates.

$$\begin{aligned}
&\frac{\delta H}{\delta \underline{x}} = -\underline{\dot{\lambda}} \\
&\frac{\delta H}{\delta r} = -\dot{\lambda}_r = \lambda_v \left[\frac{\dot{\rho}(r)}{2m} C_D A v^2 - \frac{2\mu_g}{(r+\mathrm{Re})^3} \right] \Rightarrow \dot{\lambda}_r = \lambda_v \left[-\frac{\dot{\rho}}{2m} C_D A v^2 + \frac{2\mu_g}{(r+\mathrm{Re})^3} \right], \\
&\frac{\delta H}{\delta v} = -\dot{\lambda}_v = \lambda_r - \lambda_v \frac{\rho}{m} C_D A v \Rightarrow \dot{\lambda}_v = \lambda_v \frac{\rho}{m} C_D A v - \lambda_r \\
&\frac{\delta H}{\delta m} = -\dot{\lambda}_m = \lambda_v \left[-\frac{u \cdot c}{m^2} + \frac{\rho}{2m^2} C_D A v^2 \right] \Rightarrow \dot{\lambda}_m = \lambda_v \left[\frac{u \cdot c}{m^2} - \frac{\rho}{2m^2} C_D A v^2 \right]
\end{aligned} \tag{5.5}$$

Applying transversality determines the remaining required endpoint conditions for $\lambda_{r_4}(t_f)$ and $\lambda_{v_4}(t_f)$. All other transversality conditions yield no new information and are equal to an arbitrary constant.

$$\begin{aligned}
&\bar{E} = E + \nu^T e \\
&\bar{E} = \begin{array}{c} -r_{4,f} + \nu_1 (m_{2,f} - M_1^f) + \nu_2 (m_{4,f} - M_2^f) \ldots \\ +\nu_3 (r_{1,f} - r_{2,0}) + \nu_4 (v_{1,f} - v_{2,0}) + \nu_5 (m_{1,f} - m_{2,0}) \ldots \\ +\nu_6 (r_{2,f} - r_{3,0}) + \nu_7 (v_{2,f} - v_{3,0}) + \nu_8 (m_{2,f} - m_{3,0} - M_{stage}) \\ +\nu_9 (r_{3,f} - r_{4,0}) + \nu_{10} (v_{3,f} - v_{4,0}) + \nu_{11} (m_{3,f} - m_{4,0}) \end{array} \\
&\frac{\delta \bar{E}}{\delta \underline{x}_f} = \underline{\lambda}(t_f) \\
&\frac{\delta \bar{E}}{\delta r_f} = \lambda_{r_4}(t_f) = -1 \\
&\frac{\delta \bar{E}}{\delta v_f} = \lambda_{v_4}(t_f) = 0
\end{aligned} \tag{5.6}$$

The HEE and HVC conditions yield the same result as the single stage rocket that the Hamiltonian is constant with respect to time and equal to zero.

B. FULL OPTIMAL CONTROL

The first iteration for the two-stage rocket was implemented to allow the optimal control solver to optimize the stage timing as well as the thrust profile as determined by mass flow rate. The minimum and maximum control values for each phase are listed in Table 4:

Table 4. Full Optimal Two-Stage Control Values

Phase	$u_{\min}$	$u_{\max}$
1	0	6.8
2	0	0
3	0	2.2
4	0	0

The OCP was then scaled using the scaling factors shown in Table 5:

Table 5. Full Optimal Control-Scaling Values

Scale	**Value**
L	65000
V	1000
M	10
T	1
u	1

DIDO solved the optimal control problem and generated the states and controls shown in Figure 26.

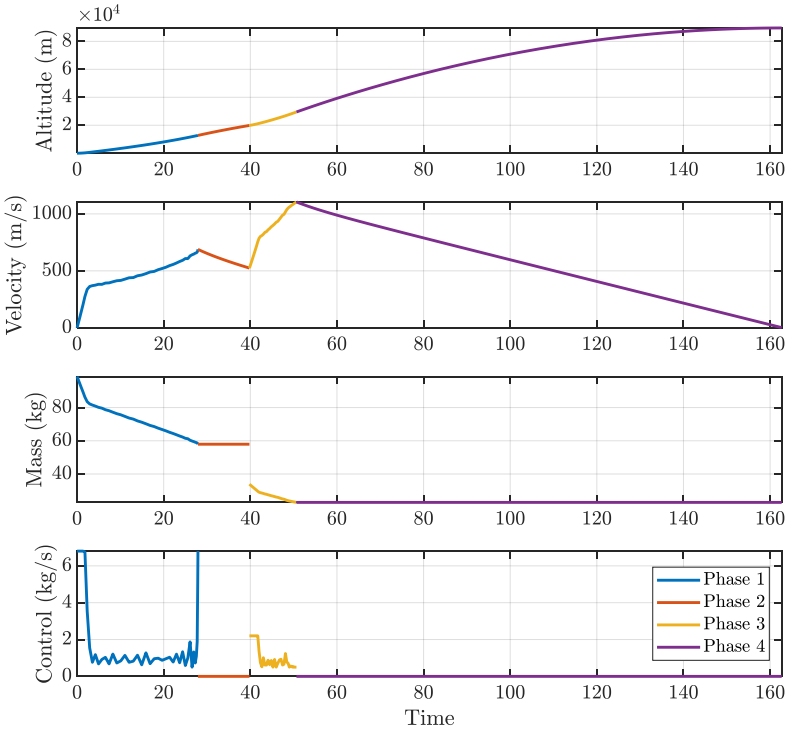

Figure 26. Two-stage Optimal Control States and Control

The simulated two-stage rocket with full optimal control of the thrust and staging achieved an altitude of 89.6 km (294,000 ft) at a max velocity of 1100 m/s.

Next, the solution must be verified and validated as an optimal control solution. First the Hamiltonian in accordance with the HVC and HEE must be constant and equal to -1. Figure 27 shows that the Hamiltonian satisfies these conditions.

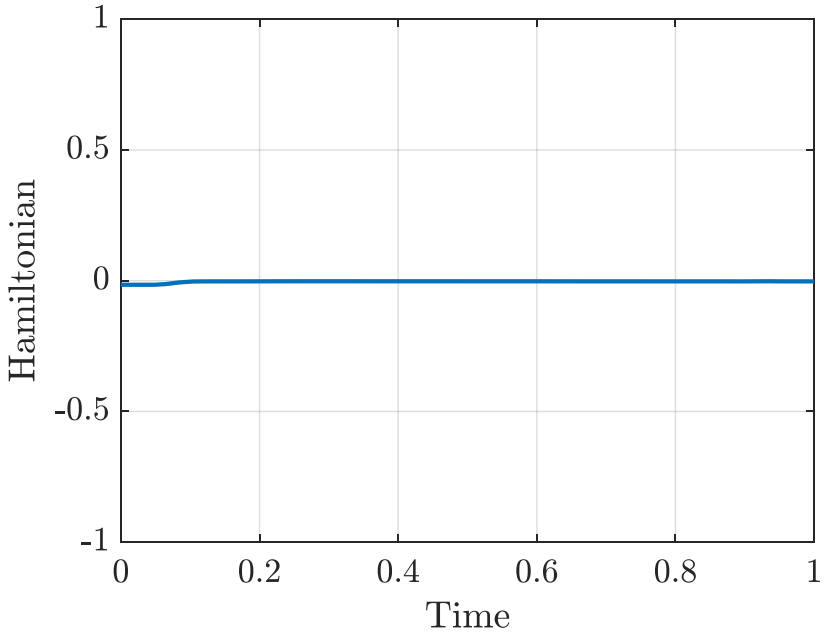

Figure 27. Two-stage Full Optimal Control Hamiltonian vs. Time

Figures 28 and 29 show that the costates are nonlinear, and λ_{r_4} and λ_{v_4} end at -1 and 0 respectively.

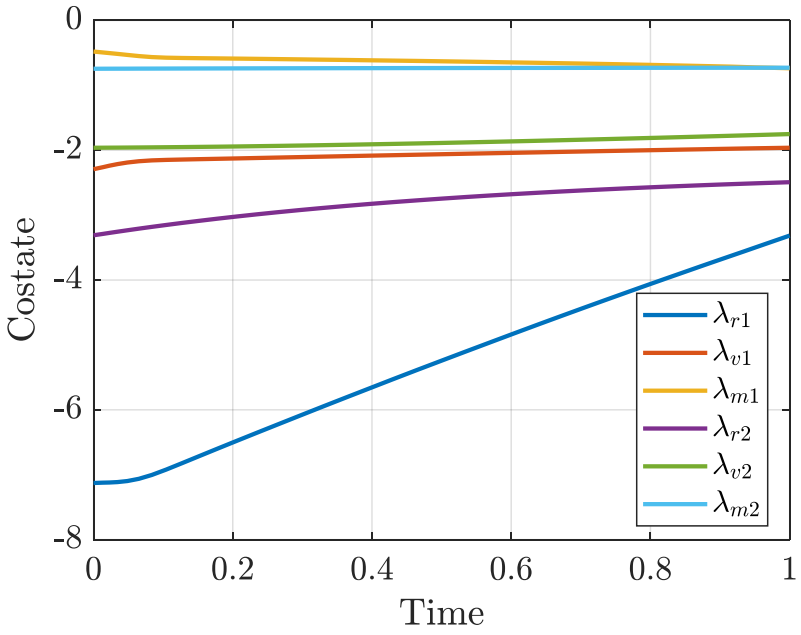

Figure 28. Two-Stage Full Optimal Control Costates vs. Time

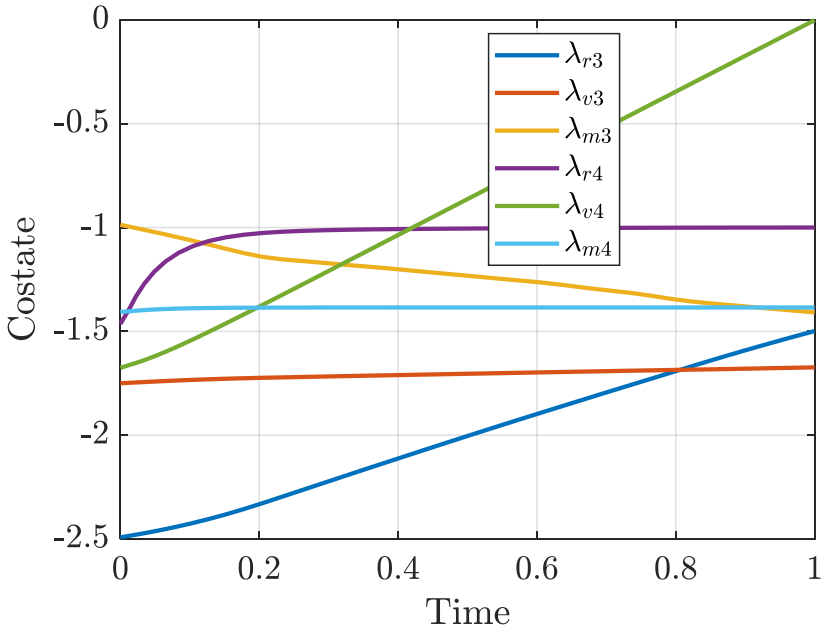

Figure 29. Two-Stage Full Optimal Control Costates vs. Time Continued

Given that the control is active only during the thrust phases, Figure 30 shows that the control behaves in accordance with the KKT Complementarity conditions.

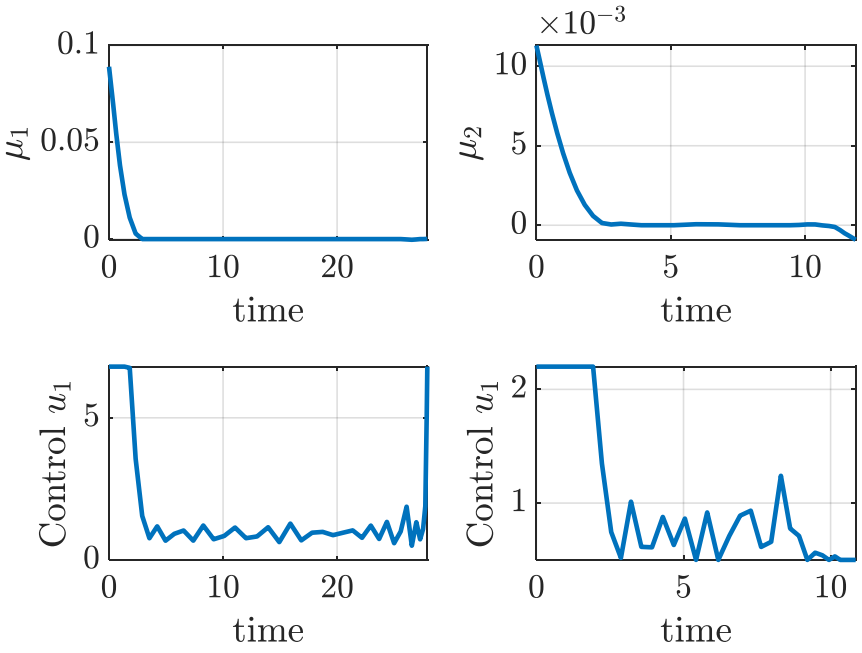

Figure 30. Two-Stage Full Optimal Control Complementarity Conditions

The last step of optimal control is to verify the feasibility of the control by propagating the control through the system dynamics. Figure 31 displays the DIDO states compared to the propagated states.

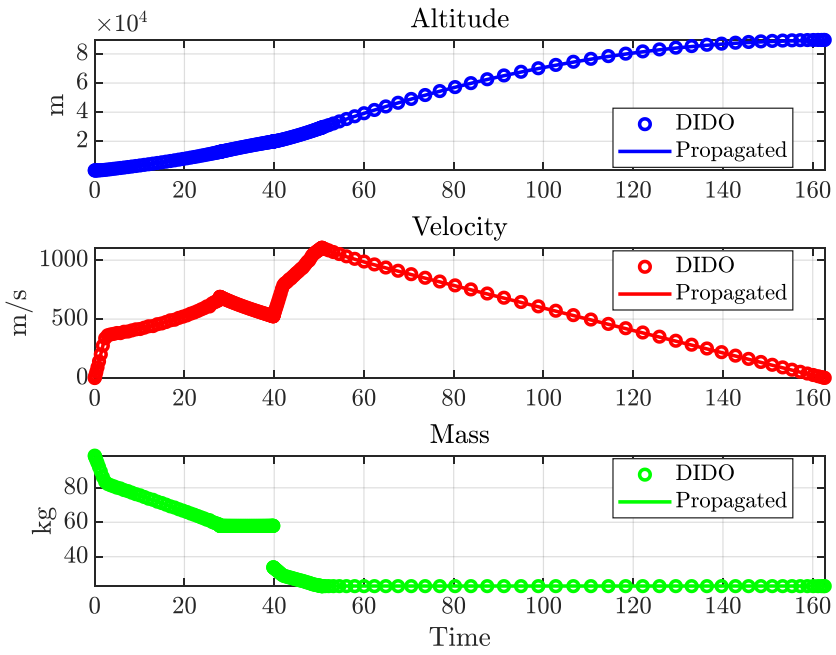

Figure 31. Two-Stage Full Optimal Control Feasibility

As shown, the DIDO optimal control of both thrust profile and stage timing meets all the verification and validation requirements as an optimal solution.

C. STAGING OPTIMAL CONTROL

Based on lessons learned from solving the single stage rocket, COTS motors can be approximated using a bang-bang style control profile. To more closely simulate these motors and determine an optimal stage timing using COTS motors, the minimum and maximum control values were adjusted and are listed in Table 6:

Table 6. Simplified Control Values

Phase	$u_{\min}$	$u_{\max}$
1	6.8	6.8
2	0	0
3	2.2	2.2
4	0	0

This change in control values required the scaling factors to be changed to achieve the most accurate results. The stage timing OCP scaling factors are listed in Table 7.

Table 7. Stage Timing Scaling Factors

Scale	Value
L	10000
V	1000
M	10
T	1
u	1

As shown in the single stage problem, the bang-bang style controller closely approximates the COTS motors. As a result, using the above control values it is possible to solve for the optimal stage timing using COTS motors. Figure 32 shows the DIDO states and controls for the timing problem.

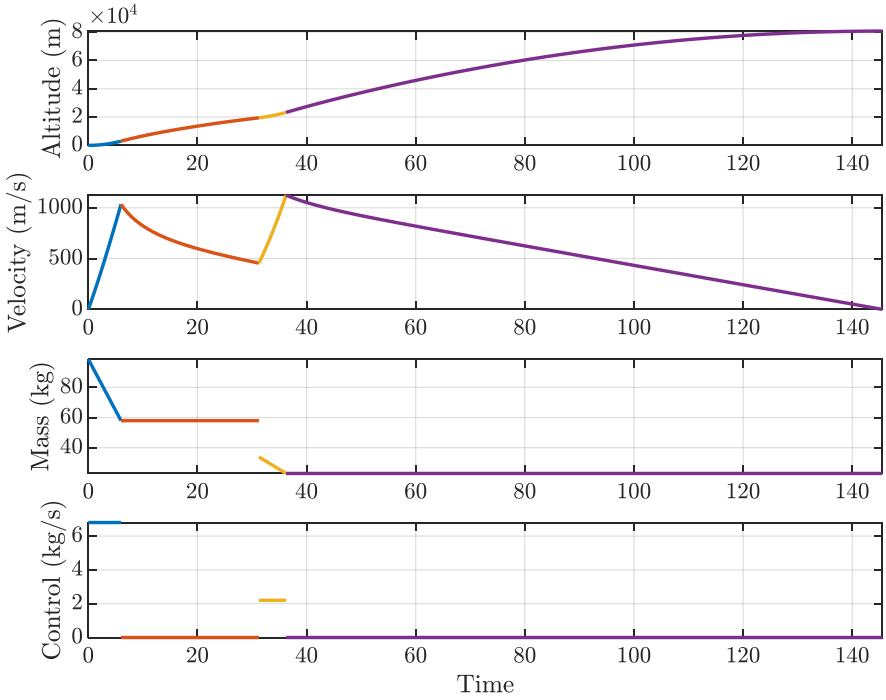

Figure 32. Two-Stage COTS Optimally Staged States and Control

As can be seen in the figure, the two-stage rocket reaches an altitude of 80.8 km (265,000 ft) with an optimal stage time of 31.27 seconds.

To test the optimality of the problem, the solution must be verified and validated using the previously listed conditions. First, Figure 33 displays that the Hamiltonian is both constant and equal to -1, satisfying the HVC and HEE.

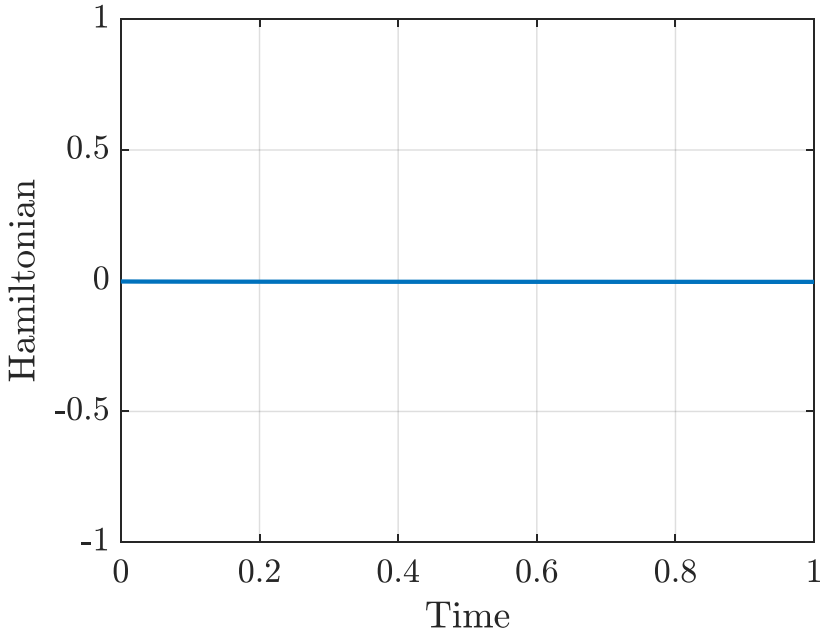

Figure 33. Two-Stage COTS Staging Hamiltonian Evolution

Next, the costates were evaluated and Figure 34 shows that λ_{r_4} and λ_{v_4} end at -1 and 0 respectively.

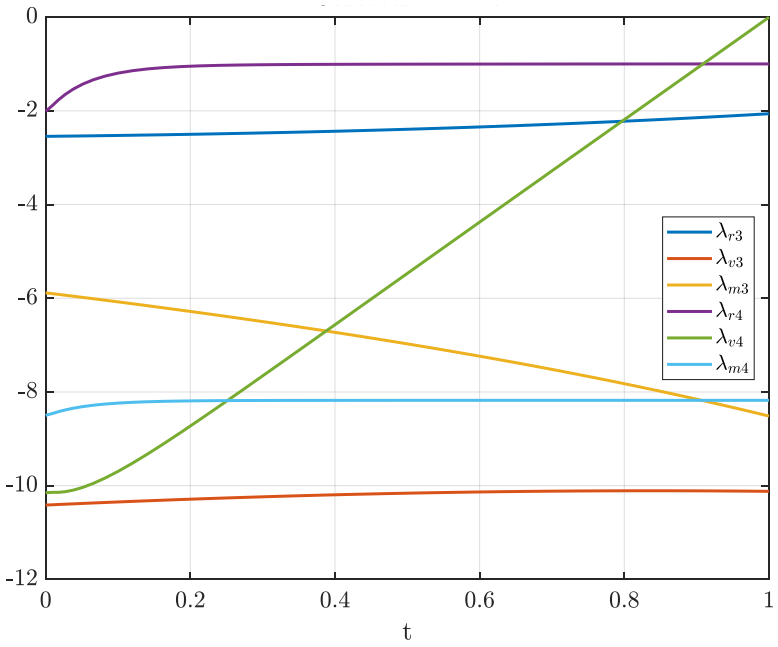

Figure 34. Two-Stage COTS Staging Costate Behavior

Then the control was propagated using the state dynamics to determine if the solution is feasible.

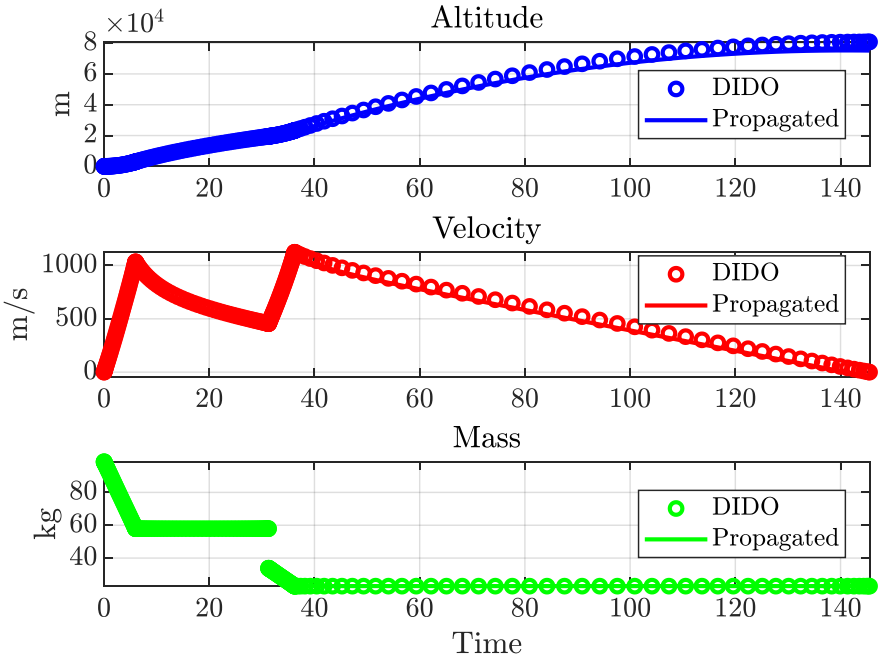

Figure 35. Two-Stage COTS Staging Feasibility

Lastly the DIDO solution was compared to utilizing the COTS Q8955 and O3400 motors for the booster and sustainer, respectively. The motor thrust profiles were utilized with the DIDO stage timing as the control for the dynamics. Figure 36 displays the flight profiles of the DIDO control as compared to the COTS motors.

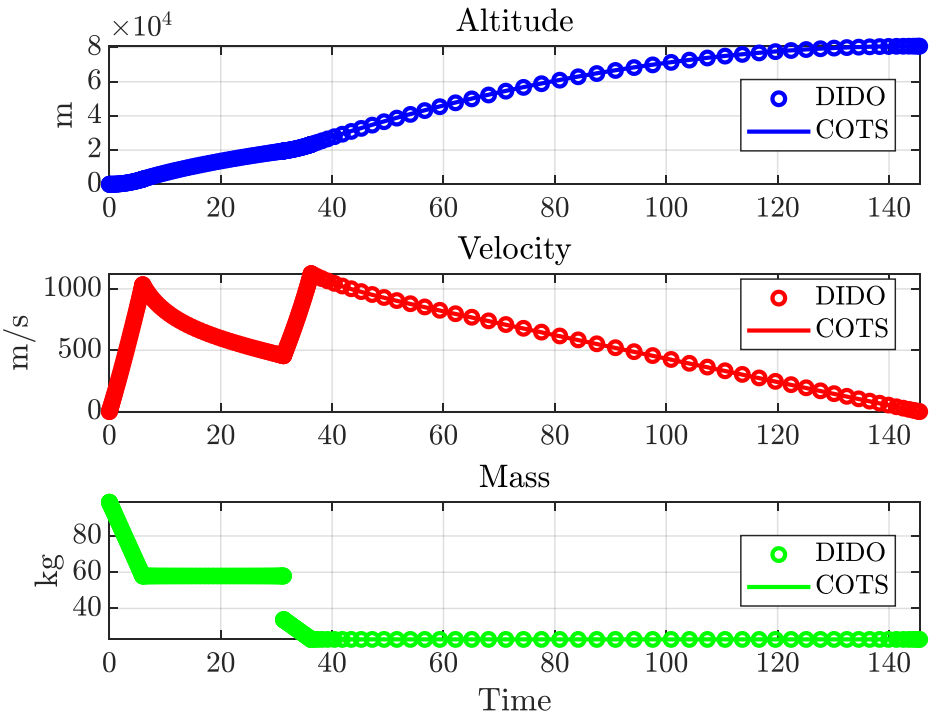

Figure 36. Two-Stage COTS Motors vs. DIDO

DIDO closely approximated utilizing the COTS motors with a difference in apogee altitude of 31 m. Next to verify the DIDO solution the dynamics were simulated using varying staging time from booster motor burnout to 40 seconds. Figure 37 shows the altitude verse staging time for this motor combination.

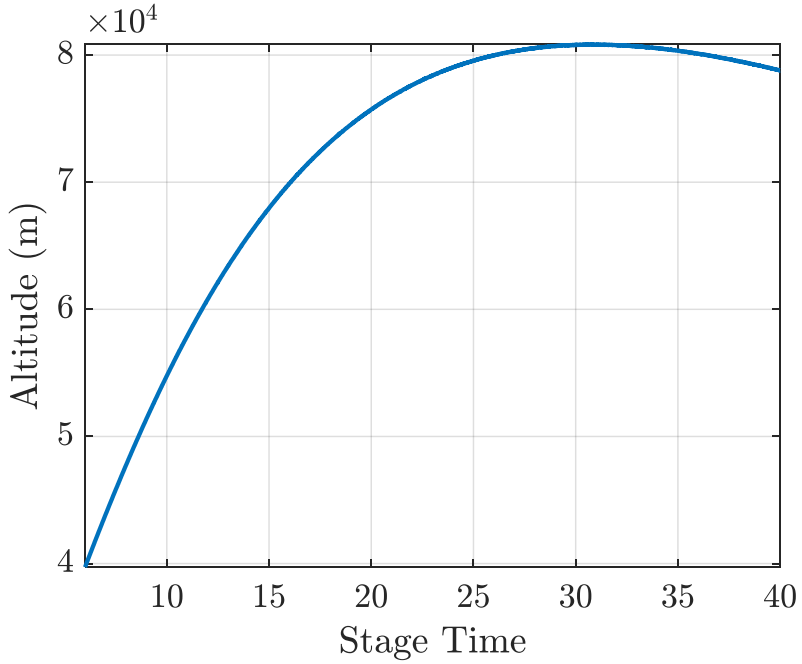

Figure 37. Stage Timing vs. Altitude

Table 8 displays the maximum altitude and stage timing for each method of solving the two-stage problem.

Table 8. Two-Stage Achieved Altitudes

Method	**Maximum Altitude (km)**	**Stage Timing (s)**
Full Optimal Control	89.6	39.79
COTS Optimal Control	80.8	31.27
Varying Stage Time	80.8	31.05

Using the propagation method, the maximum achievable altitude is 80.8 km at a staging time of 31.05 seconds. This is a difference of 0.22 seconds from the DIDO solution. One possible explanation is due to the slight differences between the DIDO solution and the COTS motors. Another source of error is long propagation time compounding numerical errors could contribute to this slight difference in optimal staging time.

The overall difference in altitudes that can be achieved by the varying staging time is primarily based on the effect of drag. Drag is proportional to the velocity squared consequently by delaying the stage timing from booster motor burnout the rocket has a lower maximum velocity and experiences less drag resistance thus achieving a greater altitude. If drag is decreased on the rocket, then the optimal stage time approaches booster motor burnout because the maximum altitude is achieved by achieving the greatest velocity.

THIS PAGE INTENTIONALLY LEFT BLANK

VI. CONCLUSIONS AND FUTURE WORK

A. CONCLUSIONS

This thesis sought to utilize optimal control theory to develop the optimal mass flow rate profile and the optimal stage timing for a two-stage rocket. Using the given wet and dry mass of a rocket as well as the motor characteristics for a given COTS rocket motor, it is possible to determine the theoretical maximum altitude of a multistage rocket ascending in one dimension. The first step of this thesis was to develop the proper fidelity for applying optimal control. It was determined that a simplified exponential atmospheric density model used in conjunction with a constant drag coefficient could produce accurate results.

Pontryagin's Principle was then applied to the optimal control problem defined during model development. The designed single stage rocket, utilizing the optimal mass flow rate, achieved an altitude of 12.7 km. However, this mass flow rate profile would be extremely difficult to manufacture and would be a custom designed motor. The COTS rocket motor thrust profile was then compared to a Bang-bang style controller that utilized the average mass flow rate to approximate the COTS thrust profile. This style mass flow profile was able to match the COTS thrust profile to within three percent of the achieved apogee altitude.

Next a two-stage rocket was simulated using both mass flow control and a fixed mass flow rate. Both these simulations were able to determine the optimal staging time for the rocket to achieve the maximum altitude. The full optimal control of the rocket motor profile achieved an altitude of 89.6 km while the simplified fixed mass flow rate achieved an altitude of 80.8 km. As proven with the single stage rocket, this is approximately the maximum achievable altitude utilizing COTS motors.

In conclusion, several different possible combination of single-stage and two-stage rockets were simulated and the optimal control theory was applied at varying levels to determine the extent that it could be applied to determine both the overall maximum

achievable altitude and the maximum altitude using COTS motors. Table 8 summarizes the altitudes above MSL achieved for each of these cases.

Table 9. Optimum Control Achieved Altitudes

Method	**Maximum Altitude (km)**
Single-Stage Optimal Control	12.7
Single-Stage COTS Motor	9.5
Two-Stage Full Optimal Control	89.6
Two-Stage COTS Optimal Control	80.8
Varying Stage Time	80.8

While it is possible to apply optimal control theory to these rockets to achieve a greater altitude than what is possible with a COTS motor, the thrust profile would make the designed motor cost prohibitive to make. It is also possible to utilize optimal control to determine the optimal stage time. However, the same result, for a one-dimensional rocket can be determined by simply propagating the dynamics repeatedly with varying stage times. This maximum altitude was determined to be achieved by delaying the ignition of the second stage to balance minimizing drag while maximizing altitude.

B. FUTURE WORK

1. Higher Fidelity Model

For this thesis work a rocket ascending in one-dimension was analyzed. Further analysis utilizing a two-dimensional model would allow for additional analysis to be conducted to include launch angle and wind effects. This would allow the model to predict achievable altitudes more accurately by including effects such as wind. Changing the launch angle has a significant effect on launch flight profile and could translate to a significant change in the mass flow model or stage time.

2. Fly Test Rockets

As part of this thesis five small two-stage rockets were procured for testing of this theory. These flights were not conducted due to time restrictions. The proposed experiment design was to utilize multiple identical rockets with varying stage timing to verify the optimal staging time determined by the optimal control solver. All the required parts and materials are on hand except for motor reloads and motor retention rings.

3. Liquid Rocket Motor

The last area of future work would be to design and build a liquid or hybrid rocket motor to test the theoretical mass flow profile determined by the optimal control solver. This in conjunction with the small two-stage rockets would be an excellent test platform to verify the theory applied in this thesis.

THIS PAGE INTENTIONALLY LEFT BLANK

LIST OF REFERENCES

[1] D. Pierce, "Development of a rocket test platform capable of delivering standard dimension payloads to near-space altitudes," M.S. thesis, Space Sys. Acad. Group, NPS, Monterey, CA, 2019. [Online]. Available: http://hdl.handle.net/10945/62696

[2] J. Yungbluth, A. Forbes, A. Writt, K. Herren, and S. Kline, "Directed study report: High Altitude balloon (HAB) experiment," Space Systems Academic Group, NPS, Monterey, CA, 2017.

[3] I. Ross and M. Karpenko, "A review of pseudospectral optimal control: From theory to flight.," *Annu. Rev. Control*, vol. 36, no. 2, pp. 182–197, Dec. 2012.

[4] I. M. Ross and F. Fahroo, "Pseudospectral knotting methods for solving nonsmooth optimal control problems," *J. Guid. Control Dyn.*, vol. 27, no. 3, pp. 397–405, May 2004, doi: 10.2514/1.3426.

[5] Federal Aviation Administration, *Code of Federal Regulations Title 14 §101*.

[6] I. M. Ross, *A primer on Pontryagin's principle in optimal control*. Carmel, CA, USA: Collegiate Publishers, 2009.

[7] R. H. Goddard, "Method of Reaching Extreme Altitudes." Aug. 26, 1920, Accessed: Jan. 03, 2020. [Online]. Available: https://search.proquest.com/congressional/view/app-gis/executive-branch/si1.7-71.2.

[8] E. Courtney, A. Courtney, and M. Courtney, "Experimental Tests of the Proportionality of Aerodynamic Drag to Air Density for Supersonic Projectiles," arXiv preprint arXiv:1510.07336, 2015 - arxiv.org

[9] P. Fossey, *RockSim*. Colorado Springs, CO, USA: Apogee Components.

[10] Community Coordinated Modeling Center, "NRLMSISE-00 Atmosphere Model." https://ccmc.gsfc.nasa.gov/modelweb/models/nrlmsise00.php (accessed Feb. 02, 2020).

[11] A. Choquette, "ThrustCurve Cesaroni O3400," *ThrustCurve Hobby Rocket Motor Search*. http://www.thrustcurve.org/motorsearch.jsp?id=1006 (accessed Feb. 19, 2020).

[12] I. M. Ross, Q. Gong, M. Karpenko, and R. J. Proulx, "Scaling and Balancing for High-Performance Computation of Optimal Controls," *J. Guid. Control Dyn.*, vol. 41, no. 10, pp. 2086–2097, Oct. 2018, doi: 10.2514/1.G003382.

[13] R. DeHate, "Q Motor Specs," Oct. 22, 2018.

THIS PAGE INTENTIONALLY LEFT BLANK

INITIAL DISTRIBUTION LIST

1. Defense Technical Information Center
   Ft. Belvoir, Virginia

2. Dudley Knox Library
   Naval Postgraduate School
   Monterey, California